ACCEPTED MANUSCRIPT

Journal of Vacuum Science & Technology A

This is the author's peer reviewed, accepted manuscript. However, the online version of record will be different from this version once it has been copyedited and typeset.
PLEASE CITE THIS ARTICLE AS DOI: 10.1116/6.0002347

Aminosilane Small Molecule Inhibitors for Area-Selective Deposition: Study of Substrate-Inhibitor Interfacial Interactions

Kaat Van Dongen[1,2], Rachel A. Nye[1,2,3], Jan-Willem J. Clerix[1,2], Claudia Sixt[1,2], Danilo De Simone[2], Annelies Delabie[1,2, a)]

[1] Department of Chemistry, University of Leuven, Leuven B-3001, Belgium

[2] IMEC, Leuven B-3001, Belgium

[3] Department of Chemical and Biomolecular Engineering, North Carolina State University, Raleigh, North Carolina 27695, USA

[a)] Authors to whom correspondence should be addressed: Annelies.Delabie@imec.be

Area-selective atomic layer deposition (AS-ALD) is a coveted method for the fabrication of next-generation nano-electronic devices as it can complement lithography and improve alignment through atomic scale control. Selective reactions of small molecule inhibitors (SMIs) can be used to deactivate growth on specific surface areas and as such enable AS-ALD. To investigate new applications of ASD, we need insight into the reactions of SMIs with a broad range of technology relevant materials. This paper investigates the reactions of aminosilane SMIs with a broad range of oxide surfaces and the impact on subsequent ALD. We compare the reactions of two aminosilane SMIs, namely dimethylamino-trimethylsilane (DMA-TMS) and hexamethyldisilazane (HMDS), with a hydroxylated SiO_2 surface and the impact on subsequent ALD processes. The DMA-TMS reaction saturates faster than the HMDS reaction and forms a dense trimethylsilyl (TMS) layer with a higher TMS surface concentration. The higher TMS surface concentration yields better inhibition and higher selectivity during subsequent TiO_2 ALD. We show that a wide range of surfaces, i.e. MgO, HfO_2, ZrO_2, Al_2O_3, TiO_2 (TiN/TiO_x), SiO_2, SnO_2, MoO_x and WO_3 remain reactive after DMA-TMS exposure for conditions where SiO_2 is passivated, indicating that DMA-TMS can enable AS-ALD on these surfaces with respect to SiO_2. On these surfaces, DMA-TMS forms residual TMS and/or

ACCEPTED MANUSCRIPT

Journal of Vacuum Science & Technology A

This is the author's peer reviewed, accepted manuscript. However, the online version of record will be different from this version once it has been copyedited and typeset.
PLEASE CITE THIS ARTICLE AS DOI: 10.1116/6.0002347

$SiO_xC_yH_z$ surface species that do not markedly inhibit ALD but may affect interface purity. Surfaces with lower, similar, and higher surface acidity than SiO_2 all show less reactivity towards DMA-TMS, suggesting that surface acidity is not the only factor affecting the substrate-inhibitor interaction. Our study also compares a hybrid inorganic-organic $SnO_xC_yH_z$ and inorganic SnO_2 material in view of their relevance as resist for EUV lithography. DMA-TMS can enable selective infiltration in $SnO_xC_yH_z$, as opposed to selective deposition on SnO_2, indicating tunable reactivity by bulk and surface composition. These insights into the reactivity of aminosilane SMIs may aid the design of new area-selective deposition processes, broaden the material space and enable new applications.

ACCEPTED MANUSCRIPT

Journal of Vacuum Science & Technology A

This is the author's peer reviewed, accepted manuscript. However, the online version of record will be different from this version once it has been copyedited and typeset.
PLEASE CITE THIS ARTICLE AS DOI: 10.1116/6.0002347

I. INTRODUCTION

Area-selective deposition (ASD) is a promising technique for the fabrication of next-generation semiconductor devices as device dimensions continue to scale down and fabrication involves ever more complex nanoscale 3D structures. ASD aims to deposit material only on specific "growth areas" of a pre-patterned substrate, while no deposition occurs on the adjacent "non-growth areas" by relying on the chemical differences between different materials. As such, ASD can be used to replicate patterns and complement conventional top-down patterning by lithography.[1,2] Atomic layer deposition (ALD) has great potential for ASD, as this deposition technique is surface dependent and provides growth control at the atomic level due to the use of self-limiting surface reactions between the gaseous precursors and a solid substrate surface.[1–5]

Selectivity can be achieved by careful tuning of the adsorption and diffusion kinetics during deposition.[1–11] Most ALD processes require activation of the growth surface or deactivation of the non-growth surface. In addition, correction steps may be used to recover from selectivity loss in the form of unintentional deposition on the non-growth area.[1-4] Deactivation approaches include amorphous polymers, self-assembled monolayers (SAMs), SAMs with modifications to enable crosslinking, and small molecule inhibitors (SMIs)[1-4,7,9,12–19]. Many papers report successful AS-ALD processes by using SAMs.[13–19,18–21,22] The surfactants that comprise the SAMs selectively bind to the non-growth surface and the long backbones (e.g., hydrophobic hydrocarbon chains) contribute to the formation of a dense, well-ordered monolayer through Van der Waals interactions. The surfactant tail groups determine the surface energy and properties of the SAM and can be designed to block adsorption of precursors during ASD. SMIs with sub-nanometer size attract recent attention as they may offer a promising approach to advance to small feature sizes in future nano-electronic device technology nodes.[7,18,19,23–25] For example, aminosilanes like dimethylamino-trimethylsilane

ACCEPTED MANUSCRIPT
Journal of Vacuum Science & Technology A
This is the author's peer reviewed, accepted manuscript. However, the online version of record will be different from this version once it has been copyedited and typeset.
PLEASE CITE THIS ARTICLE AS DOI: 10.1116/6.0002347

(DMA-TMS, Fig. 1a) can be used to deactivate SiO_2 during AS-ALD.[7,24, 25,26,27] DMA-TMS reacts with Si-OH surface groups according to the following equation:

$$Si-OH\ (s) + (CH_3)_2\mathrm{NSi(CH_3)_3}\ (\mathrm{g}) \rightarrow Si-O-Si(CH_3)_3\ (\mathrm{s}) + \mathrm{NH(CH_3)_2}\ (g)$$

The DMA-TMS reaction on a fully hydroxylated SiO_2 surface at 250°C forms a surface termination with densely packed trimethylsilyl (TMS) groups.[7] The resulting surface hydrophobicity and low concentration of reactive OH surface sites inhibit ZrO_2, TiO_2, TiN and Ru ALD.[7,9,27,28] Different SMIs may be combined to improve selectivity.[27,28] For example, the inhibition of Al_2O_3 ALD was improved by performing Bis(N,N-dimethylamino)-dimethylsilane ((B)DMADMS, Fig. 1b) and DMA-TMS treatments in sequence before the ALD process.[28] Hexamethyldisilazane (HMDS, Fig. 1c) could be an interesting SMI as it contains two TMS groups that can potentially react according to the following equations:[29,30]

$$Si-OH\ (s) + H\mathrm{N(Si(CH_3)_3)_2}\ (\mathrm{g}) \rightarrow Si-O-Si(CH_3)_3\ (\mathrm{s}) + \mathrm{H_2N}Si(\mathrm{CH_3})_3\ (g)$$

$$Si-OH\ (s) + H_2\mathrm{NSi(CH_3)_3}\ (\mathrm{g}) \rightarrow Si-O-Si(CH_3)_3\ (\mathrm{s}) + \mathrm{H_3N}\ (\mathrm{g}).$$

While studies have compared the properties of DMA-TMS and HMDS treated SiO_2 surfaces[31,32,33,34], their inhibiting performance in the context of AS-ALD has not yet been compared. More generally, limited understanding exists about SMIs and compatibility with ALD processes.[18] Due to their small size, the selectivity critically depends on the interface between substrate and inhibitor and the interface between inhibitor and ALD precursors.[18] Better understanding of the substrate-inhibitor interfacial interactions is therefore essential to improve the selectivity of AS-ALD processes with SMIs and may contribute to rational design of SMIs for AS-ALD.[18] For SMIs to be effective in ASD applications, they must react selectively with the non-growth surface without affecting the growth surface. Indeed, DMA-TMS is less reactive towards TiN, TiO_2 and Ru compared to SiO_2. These materials can act as growth surfaces in ASD applications with SiO_2 as the non-growth surface.[25] To enable new applications of ASD such as patterning in nano-electronic device fabrication, we need to

ACCEPTED MANUSCRIPT
Journal of Vacuum Science & Technology A
This is the author's peer reviewed, accepted manuscript. However, the online version of record will be different from this version once it has been copyedited and typeset.
PLEASE CITE THIS ARTICLE AS DOI: 10.1116/6.0002347

understand the reactions of SMIs with a broad range of technology relevant materials. Of great value are insights in various factors that govern the surface-SMI interactions to possibly predict compatibility of substrates and SMIs. Factors that can play a role are surface acidity, surface composition and stoichiometry, OH density and H-bonding of OH groups, surface roughness, phase, and catalytic properties, among others.

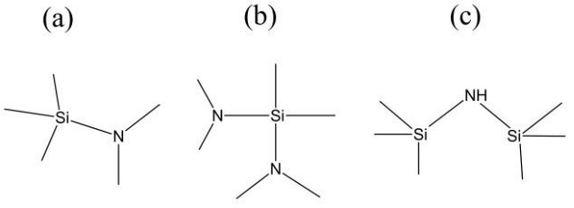

FIG. 1. Structure of (a) DMA-TMS, (b) (B)DMADMS and (c) HMDS.

In this work, we therefore investigate substrate-inhibitor interfacial interactions for oxide surfaces and aminosilane SMIs. First, we compare the reactions of HMDS and DMA-TMS on hydroxylated SiO_2 surfaces and explore the impact on the selectivity of TiO_2 ($TiCl_4/H_2O$) and TiN ($TiCl_4/NH_3$) ALD. We vary temperature and exposure time of the SMIs to achieve the maximum TMS surface concentration and study the impact on the subsequent ALD process. Next, we explore the reactivity of DMA-TMS towards various metal oxide surfaces, to seek insight in how surface properties affect the reaction with DMA-TMS as well as the subsequent ALD process. We analyze the potential impact of surface acidity for a broad range of materials including MgO, HfO_2, ZrO_2, Al_2O_3, TiO_2 (TiN/TiO_x), SiO_2, SnO_2, MoO_x, WO_3 (in order of increasing Sanderson surface acidity). Our study also compares a hybrid inorganic-organic $SnO_xC_yH_z$ with the inorganic SnO_2 material in view of their relevance as resist for EUV lithography.

II. EXPERIMENTAL

A Materials and Processing

ACCEPTED MANUSCRIPT
Journal of Vacuum Science & Technology A
This is the author's peer reviewed, accepted manuscript. However, the online version of record will be different from this version once it has been copyedited and typeset.
PLEASE CITE THIS ARTICLE AS DOI: 10.1116/6.0002347

Silicon oxide (SiO_2) substrates were prepared by plasma-enhanced atomic layer deposition (PEALD) of 17 nm SiO_2 on a 1mm thick 300 mm Si(100) wafer in an ASM Eagle 12 reactor at 75 °C. The PEALD cycle consisted of a Si precursor pulse, a purge, exposure to O_2 plasma and a final purge. The resulting SiO_2 surface contains ~2.5 OH sites/nm^2.[25] We note that the OH content of all other considered surfaces is difficult to quantify and it can therefore not be reported.

SnO_2 and $SnO_xC_yH_z$ (x>1) substrates were prepared by spin coating of a proprietary Inpria Corp solution of a Sn-based metal oxide material on a TEL track, on the 100 nm PEALD SiO_2 layer, followed by UV exposure of 27 mJ/cm^2 in N_2 atmosphere and hard bake. The resulting spin-coated film is 22 nm thick. To obtain $SnO_xC_yH_z$ (x>1), the hard bake was performed at 180 °C for 60 s and to achieve SnO_2, the hard bake was done at 450 °C for 30 minutes according to the equations:

$$SnO_XL_N \xrightarrow{UV + 180°C\ 60\ s} SnO_XL_{N-M} \qquad (L = C_YH_Z)$$

$$SnO_XL_N \xrightarrow{UV + 450°C\ 30\ min} SnO_2$$

The thickness of the $SnO_xC_yH_z$ (x>1) and SnO_2 layers were 8.9 nm and 5 nm, respectively.

Mo and MgO were deposited through physical vapor deposition (PVD) in a Canon-Anelva EC7800 tool. The thickness of the Mo and MgO layers were 20 nm and 22 nm, respectively. For MgO PVD, the chamber pressure was ~10^{-9} Torr. MgO deposition was performed using radio frequency at a deposition rate <0.1 Å/s and Ar as purge gas with a pressure of ~10^{-5} Torr. HfO_2, Al_2O_3 and ZrO_2 ALD were performed in an ASM XP4 tool at 300 °C. A full ALD cycle consisted of a saturated metal precursor dose ($HfCl_4$, $Al(CH_3)_3$ (trimethylaluminum or TMA) and $ZrCl_4$, respectively), a purge, a saturated H_2O reaction and a final purge. The resulting metal oxide layers were 20 nm thick. W ALD was performed in a Centura-3 tool on top of a TiN underlayer. The W ALD layers are 5 nm thick.

ACCEPTED MANUSCRIPT
Journal of Vacuum Science & Technology A
This is the author's peer reviewed, accepted manuscript. However, the online version of record will be different from this version once it has been copyedited and typeset.
PLEASE CITE THIS ARTICLE AS DOI: 10.1116/6.0002347

The HMDS reaction was performed in a TEL track tool. The wafer was transferred to the reactor and set on top of a hot plate kept at 135 °C or 180 °C. After evacuating the chamber, the chamber was filled with N_2 gas and HMDS through a showerhead up to a total pressure of 35 Torr, with the exhaust off. After the static exposure time (15 s to 1200 s), the exhaust was activated to remove HMDS molecules and achieve atmospheric pressure under N_2. The DMA-TMS reaction took place in a TEL Tactras chamber at 5 Torr in a N_2 environment for varying times at 135 °C, 180 °C or 250 °C. After placing the wafer on the chuck, the chamber was filled with N_2 (500 sccm) to a pressure of 5 Torr. After remaining at these conditions for 15 minutes, the pressure was reduced to 1-3 mTorr. Then, a gaseous mixture of N_2 (350 sccm) and DMA-TMS (500 sccm) was introduced, reestablishing a pressure of 5 Torr. The wafer was kept at these conditions at the set temperature for desired DMA-TMS dose duration (5 s to 1140 s). For the combined HMDS/DMA-TMS treatment, the wafer was first transferred to the TEL Lithius proZ chamber for the HMDS reaction at 180 °C (150 s to 300 s) followed by a transfer to the TEL Tactras chamber for the DMA-TMS reaction at 250C° (150 s to 300 s), following the same procedure as described in the previous paragraphs for each inhibitor.

TiO_2 and TiN ALD were performed in an ASM Polygon 8300 EmerALD showerhead-type ALD chamber. The TiO_2 films were deposited with $TiCl_4/H_2O$ ALD and 5 Torr using ALD cycles that demonstrate self-limiting growth on SiO_2 substrates. The wafer chuck was heated to 150 °C, while the walls and showerhead were kept at 125 °C. The TiN films were deposited at ~2 Torr with $TiCl_4/NH_3$ ALD using ALD cycles that demonstrate self-limiting growth on SiO_2 substrates. The chuck was heated to 300 °C or 390 °C, while the chamber walls and showerhead were kept at 160 °C. For some experiments, we investigated the impact of the ALD temperature by varying the wafer chuck temperature between 125 and 370°C. Depositions at temperatures lower than 125°C cannot be performed as the reactor temperature needs to be significantly higher than the $TiCl_4$ precursor evaporation temperature to avoid

ACCEPTED MANUSCRIPT
Journal of Vacuum Science & Technology A
This is the author's peer reviewed, accepted manuscript. However, the online version of record will be different from this version once it has been copyedited and typeset.
PLEASE CITE THIS ARTICLE AS DOI: 10.1116/6.0002347

condensation that compromises ALD behavior and causes particle issues. Experiments for TiN ALD at temperatures lower than 300°C are impractical due to slow reaction kinetics. Experiments at temperatures higher than 390°C cannot be performed with the current ALD tool. The residual Cl-content in TiO_2 films deposited between 125 and 150°C is below 1 atomic% according to X-ray Photoelectron Spectroscopy (XPS). The Cl-content in the TiO_2 films deposited between 200 and 300°C was below the detection limit of XPS.

The wafers were stored in clean room air for several days between deposition of the oxide or metal, the treatment of the SMI and the TiO_2 or TiN ALD. Mo and W surfaces oxidize during air exposure, as evidenced by XPS (see results). These samples are therefore referred to as Mo/MoO_x and W/WO_3. Storage in air may result in slow collection of organic contamination on the sample surfaces. This is not expected to influence the experiments as we applied a pre-stabilization step to desorb the organic contamination before the adsorption of the SMI and before the TiO_2 or TiN ALD.

B Characterization

The metal(loid) oxide surfaces were characterized before and after SMI treatment using water contact angle (WCA) measurements and X-ray photoelectron spectroscopy (XPS). WCA measurements were done on a Dataphysics OCAH 230L tool in sessile drop mode, using 1 µL droplets of deionized water. SCA20 software was used to analyze the droplets using Laplace-Young fitting. The WCA measurement was repeated at least 5 times for each sample. The reported values are the average of at least 5 measurements. The error bars on the figures represent the error as the sum of the standard deviation and the averaged error of the fit per droplet as given by the SCA20 software. Conclusions are only drawn from repeated measurements.

The XPS spectra for DMA-TMS and HMDS passivation on SiO_2, SnO_2 and $SnO_xC_yH_z$ ($x>1$) were conducted in angle resolved mode (and angle integrated for SnO_2/ $SnO_xC_yH_z$ ($x>1$))

ACCEPTED MANUSCRIPT
Journal of Vacuum Science & Technology A
This is the author's peer reviewed, accepted manuscript. However, the online version of record will be different from this version once it has been copyedited and typeset.
PLEASE CITE THIS ARTICLE AS DOI: 10.1116/6.0002347

on a Thermo instruments Theta300 spectrometer. The spectra were recorded using an Al Kα X-ray source with an energy of 1486.6 eV and a 100 μm spot size. The angle was varied between 69° and 12° from the surface of the sample (=take off angle, TOA), with smaller angles giving more surface sensitive information. The XPS spectra for samples after DMA-TMS reaction on the metal oxides were recorded on different instruments and with varying settings. The Si2p spectra at a 20° TOA, and corresponding Si-content, for a 300 s DMA-TMS dose on HfO_2, WO_3 and MoO_x was measured in angle integrated mode on a Versaprobe 3 from Physical electronics, while the Mo3d, and HfO_2 C1s spectra for 0 s and 1800 s DMA-TMS reaction were measured in angle integrated mode on a QUANTES instrument from Physical electronics at a 70° TOA. The Si2p spectra at both 20° and 70° TOA and corresponding Si-content for 0 s, 300 s and 1800 s on MgO, Al_2O_3 and ZrO_2 were obtained on the same QUANTES instrument, but in angle resolved mode. All XPS analyses used a monochromatized photon beam of 1486.6 eV (Al Kα source), a 100 μm spot and charge neutralization.

To enable qualitative comparisons of XPS data, the Si-content was estimated using a surface contamination model, as described previously.[7,25] The Si-content was considered as sub-monolayer thickness and the surface concentration was estimated from equation 1 with n_x the surface concentration, I_x and I_{sub} the intensities of the species and substrate, respectively, l_{sub} the electron attenuation length for quantitative analysis, and N_{sub} the atomic concentration in the substrate (based on the molar volume given at WebElements). Sensitivity factors specific for each instrument were used to convert peak areas to atomic concentrations. As a result of this, it is possible that the concentrations deviate from reality in the absolute sense (generally 10-20% relative). Given these assumptions, the estimated surface concentrations are solely used for qualitative and relative comparisons.

$$n_x = \frac{I_x}{I_{sub}} * l_{sub} * N_{sub} \qquad \text{Equation 1}$$

ACCEPTED MANUSCRIPT
Journal of Vacuum Science & Technology A
This is the author's peer reviewed, accepted manuscript. However, the online version of record will be different from this version once it has been copyedited and typeset.
PLEASE CITE THIS ARTICLE AS DOI: 10.1116/6.0002347

The Ti content after TiO_2 and TiN ALD on the untreated and SMI-treated metal(loid) substrates was studied with Rutherford backscattering spectrometry (RBS) using a 6SDH Pelletron from National Electrostatics Corporation, a scattering chamber from Jülich Research Center and an Arun Microelectronics Ltd. multi axis goniometer. This setup uses a 1.523 MeV He^+ incoming ion beam, at a 170° scattering angle, a 11° tilt angle and a 20 nA beam current to quantify the Ti content on the surface. The silicon surface barrier detector was calibrated considering offset, gain and full width at half maximum. The RBS analysis has a detection limit of ~10^{13} atoms/cm^2. The obtained spectra were analyzed with SA-numeric integration and plots were made with Arriba. The overall uncertainty in the Ti atom measurements by RBS is less than 1×10^{15} atoms/cm^2. All figures include error bars that indicate the uncertainly in Ti content. In some cases, the error bar is smaller than the datapoint symbol and therefore not visible. The TiO_2 or TiN thickness were calculated based on the RBS Ti areal density assuming a bulk density of 4.23 and 5.22 g/cm^3, respectively.

To determine the OH concentration on a PEALD SiO_2 substrate, it was exposed to a $HfCl_4$ (300 °C) pulse in a XP4 chamber, followed by quantification of Hf with (RBS). It can be assumed that the Hf concentration is equal to the number of OH sites on the surface.[7,35]

TiO_2 and TiN growth were visualized using scanning electron microscopy (SEM) on a FEI Helios 460 microscope with 3kV beam energy and 100 pA beam current for TiO_2 and using a Hitachi SU8000 instrument with 3kV voltage and 10 pA beam current for TiN. In addition, transmission electron microscopy (TEM) images were taken for a more detailed visualization of the TiN distribution using a FEI Tecnai F30 ST setup. The setup used a field emission gun (FEG) electron source operated at 300 kV. The samples were prepared by coating the top with spin-on carbon before a focused ion beam lift-out (5 kV) on a Helios 450 HP tool. Images were acquired in TEM and scanning TEM mode. Some experiments also utilized energy dispersive X-ray spectroscopy (EDS) analysis.

ACCEPTED MANUSCRIPT
Journal of Vacuum Science & Technology A
This is the author's peer reviewed, accepted manuscript. However, the online version of record will be different from this version once it has been copyedited and typeset.
PLEASE CITE THIS ARTICLE AS DOI: 10.1116/6.0002347

Atomic force microscope (AFM) measurements of the initial surfaces were recorded with a Bruker ICON PT tool with Nanoscope V controller and a OCML-AC160TS tip (nominal tip radius: 7-9 nm) in tapping mode. Scan areas of 5x5 μm and 1x1 μm were recorded. The root mean square (RMS) average of height deviation was calculated from the mean image data plane.

III. RESULTS AND DISCUSSION

A. Reaction of DMA-TMS and HMDS with SiO_2 substrates

We first study the surface reactions of DMA-TMS and HMDS on a hydroxylated SiO_2 substrate. Our goal is to understand the conditions that lead to a densely packed TMS layer that can effectively block precursor adsorption during ALD. We investigate various SMI reaction times (0-1200 s) and temperatures (135 °C, 180 °C and 250 °C). The TMS surface concentration is studied using WCA and XPS measurements. WCA measurements are commonly used to study the extent of surface modification by SMI.[18] The change in WCA by adsorption of the SMI on the surface relates to the change in surface energy and gives an indication of the surface coverage of the SMI on the surface. Indeed, we have previously shown correlations between WCA values and XPS TMS surface concentrations on SiO_2 substrates.[7,25] The results are shown in Fig. 2.

The initial hydrophilic SiO_2 surface is characterized by a WCA between 6 and 23 ° due to varied levels of organic contaminants (Fig. 2).[25] The surface becomes more hydrophobic after reaction with the SMIs, indicated by higher WCAs. All reactions are self-limiting: the WCA increases with increasing SMI exposure time and eventually saturates (Fig. 2a). The time required to achieve saturation and the WCA value at saturation are clearly different for the HMDS and DMA-TMS reactions. At 135 °C, the DMA-TMS reaction saturates after 300 s and the WCA becomes 97°, indicating that a dense layer of TMS groups is quickly formed. In contrast, at the same temperature, the HMDS reaction saturates only after 600 s and the WCA

ACCEPTED MANUSCRIPT
Journal of Vacuum Science & Technology A
This is the author's peer reviewed, accepted manuscript. However, the online version of record will be different from this version once it has been copyedited and typeset.
PLEASE CITE THIS ARTICLE AS DOI: 10.1116/6.0002347

becomes 80°. This demonstrates that the HMDS reaction is slower and eventually results in a lower TMS surface concentration.

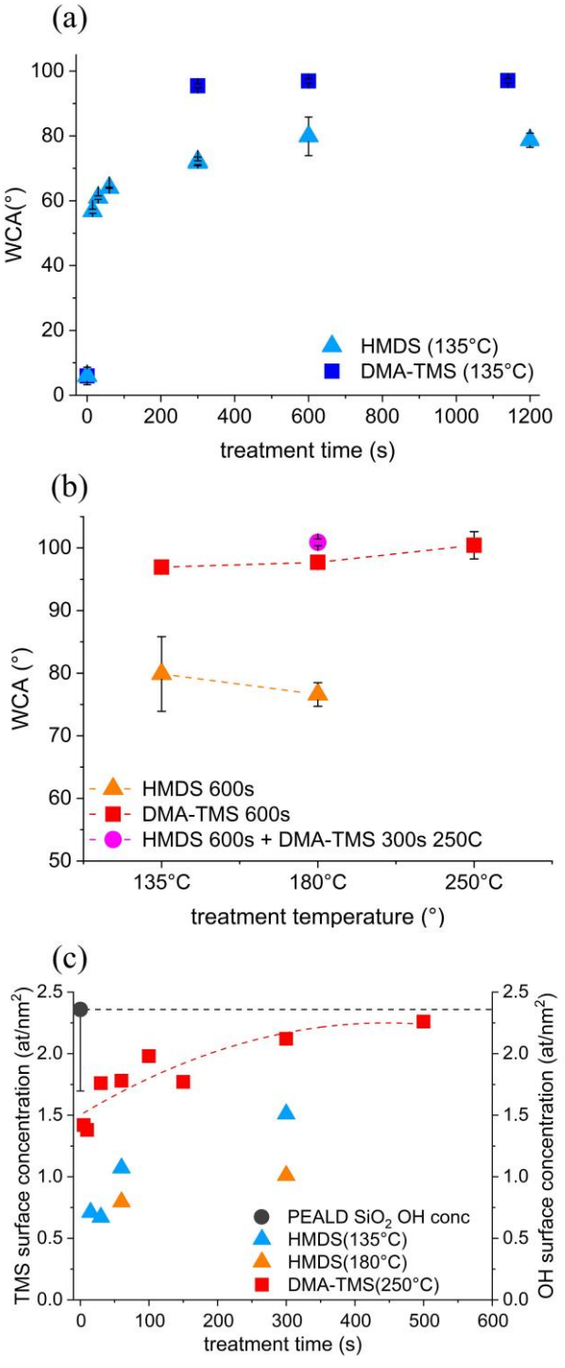

FIG. 2. (a) Impact of DMA-TMS and HMDS treatment (135 °C) on the SiO_2 WCA. (b) Impact of aminosilane treatment temperature on the SiO_2 WCA. (c) The change in TMS concentration (estimated by XPS) after DMA-TMS and HMDS reaction. The dashed lines are provided as guide to the eye.

ACCEPTED MANUSCRIPT
Journal of Vacuum Science & Technology A
This is the author's peer reviewed, accepted manuscript. However, the online version of record will be different from this version once it has been copyedited and typeset.
PLEASE CITE THIS ARTICLE AS DOI: 10.1116/6.0002347

The temperature has a minor impact on the final surface composition after the DMA-TMS and HMDS reactions (Fig. 2b). For the HMDS reaction, the WCA values at saturation increase slightly when we increase the temperature from 135 to 250 °C. For the DMA-TMS reaction, we obtain similar WCA values between 97 and 100° for the reactions at 135, 180, and 250 °C. The WCA after HMDS treatment is substantially lower as compared to the DMA-TMS reaction at each temperature considered here (e.g. 77 º at 180°C). It may be possible to further increase WCA by increasing the temperature or substantially extending the HMDS exposure times, but the latter becomes impractical.[34] Surfaces treated by sequential exposures of HMDS and DMA-TMS at 180 ºC show a similar WCA as for the single DMA-TMS reaction. Thus, the combination of these SMIs does not help to increase the TMS surface concentration.

The WCA results are consistent with the trends in TMS concentrations from XPS (Fig. 2a and c). The Si atoms in TMS groups have a different oxidation state compared to the Si atoms in the SiO_2 layer, resulting in a different binding energy (BE) in the Si2p XPS spectra for TMS groups (101-101.5 eV) and bulk SiO_2 (103-103.5eV).[7,25] TMS concentrations are estimated based on a surface contamination model using an ideal 2D hexagonally close packing (Experimental, as detailed previously[7,25]). The qualitative trends from XPS confirm the self-limiting nature of the DMA-TMS reaction. Furthermore, XPS indicates that TMS surface concentrations after the HMDS reaction are lower as compared to TMS surface concentrations after the DMA-TMS reaction. The lower TMS surface content after HDMS reaction is consistent with a previous study from Imada et al.[33] They compared the trimethylsilyl (TMS) surface coverage for aminosilane treatments at 110 °C by analyzing the electrical permittivity and the leakage current and by analyzing infrared measurements. The lower TMS surface content after HMDS reaction as compared to DMA-TMS was linked to the higher boiling point and lower partial pressure. In contrast, similar TMS surface concentrations were obtained for DMA-TMS and HMDS treatments at higher temperature (280 °C) in a closed container.[34]

ACCEPTED MANUSCRIPT
Journal of Vacuum Science & Technology A
This is the author's peer reviewed, accepted manuscript. However, the online version of record will be different from this version once it has been copyedited and typeset.
PLEASE CITE THIS ARTICLE AS DOI: 10.1116/6.0002347

B. Effect of DMA-TMS and HMDS treatment on SiO_2 on the ALD growth

Next, we investigate the impact of the DMA-TMS and HMDS pretreatments on growth evolution during TiO_2 ALD at 150 °C by RBS and SEM. The RBS results are shown in Fig. 3. To enable comparison, we calculate the selectivity as the normalized difference in surface coverage between the growth and the non-growth surface, as given in equation 2[2,3,4,7,25,36,37] (Fig. 3b).

$$S = \frac{(\theta_G - \theta_{NG})}{(\theta_G + \theta_{NG})} \sim \frac{(t_G - t_{NG})}{(t_G + t_{NG})} \qquad \text{Equation 2}$$

In this formula, S represents selectivity, and θ_G and θ_{NG} (t_G and t_{NG}) represent surface coverage (or thickness) on the growth and non-growth surface, respectively. As approximation, we use the Ti content (at/cm^2) or thickness from RBS instead of surface coverage. In addition, particle growth on the different substrates is visualized using SEM.

HMDS pretreatment (135 °C for 300 s) only slightly affects the TiO_2 growth behavior on SiO_2 (Fig. 3a). We obtain 2.6 nm TiO_2 after 100 ALD cycles on the HMDS treated SiO_2, as compared to 3.4 nm on untreated SiO_2 substrate. This suggests that the TMS concentration (~1-1.5 TMS groups/nm^2) after HMDS reaction is insufficient to passivate the SiO_2 substrate and has only minor impact on the TiO_2 ALD. The resulting selectivity is only 0.13 for a TiO_2 film thickness of ~3.4 nm on the SiO_2 growth surface (Fig. 3b). In contrast, the DMA-TMS-treated surface (at 135 °C for 300 s) substantially delays TiO_2 growth: we observe only ~ 0.17 nm TiO_2 after 100 ALD cycles, which corresponds to a selectivity of 0.90. The selectivity does not change significantly when the temperature of the DMA-TMS reaction is increased from 135 to 250°C, in line with the similar WCA values (97 - 100°) that indicate similar TMS-concentrations. The difference in selectivity between DMA-TMS and HMDS is in line with the difference in WCA and TMS surface coverage from XPS as described above: the higher the TMS concentration, the higher the selectivity. In addition, we study the impact of sequential HMDS and DMA-TMS reactions on the TiO_2 growth. The combination has no major impact

ACCEPTED MANUSCRIPT
Journal of Vacuum Science & Technology A
This is the author's peer reviewed, accepted manuscript. However, the online version of record will be different from this version once it has been copyedited and typeset.
PLEASE CITE THIS ARTICLE AS DOI: 10.1116/6.0002347

on the growth delay, in line with the similar TMS concentrations for both conditions. A selectivity of 0.95 is found for ~3.4 nm TiO_2 deposition on untreated SiO_2, close to the value for a single DMA-TMS reaction.

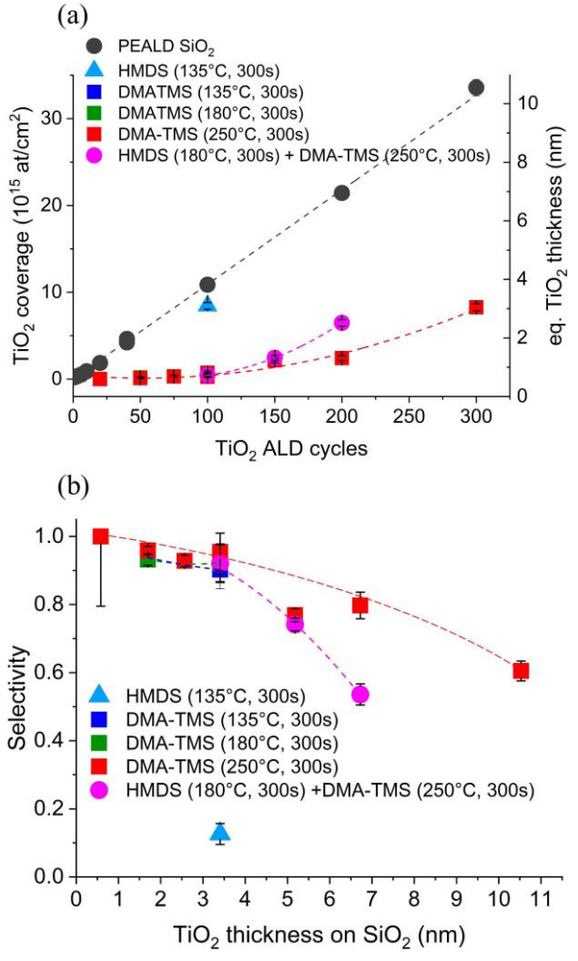

FIG. 3. (a) TiO_2 growth ($TiCl_4/H_2O$ ALD, 150 °C) on untreated SiO_2 and, DMA-TMS-, HMDS- and DMA-TMS/HMDS-treated SiO_2 (b) $TiCl_4/H_2O$ ALD selectivity for untreated SiO_2 as the growth surface and the DMA-TMS/HMDS treated SiO_2 as non-growth surface. The dashed lines are provided as guide to the eye. The reported error bars on the TiO_2 coverage and selectivity are determined through error propagation based on the uncertainties of the RBS measurements (experimental details).

The morphology of the deposited TiO_2 was analyzed with SEM after 100 and 300 cycles of TiO_2 ALD at 150 ºC on three surfaces with different TMS content, namely untreated SiO_2, SiO_2 treated with 300 s DMA-TMS at 250 °C, and SiO_2 treated with 300 s HMDS at 135 °C.

ACCEPTED MANUSCRIPT
Journal of Vacuum Science & Technology A
This is the author's peer reviewed, accepted manuscript. However, the online version of record will be different from this version once it has been copyedited and typeset.
PLEASE CITE THIS ARTICLE AS DOI: 10.1116/6.0002347

The results are shown in Fig. 4. SEM reveals a clearly different TiO_2 morphology for the different substrates, indicating that the TiO_2 ALD growth mode depends on the TMS surface concentration. On the untreated SiO_2 layer, we observe a smooth TiO_2 layer that completely covers the SiO_2 substrate (Fig. 4a). When HMDS is used as SMI, we observe a high number of individual as well as coalesced TiO_2 nanoparticles on the substrate, indicating partial TiO_2 coverage, in line with the lower TMS surface content (WCA and XPS) (Fig. 4b). The partial TiO_2 surface coverage could be due to a non-uniform distribution of TMS groups on the SiO_2 substrate after the HMDS reaction, where areas with a higher TMS content locally block the surface for adsorption during TiO_2 ALD, resulting in the minor nucleation delay observed from RBS (Fig. 3a). However, overall, the TMS surface concentration (WCA and XPS) is too low to fully block adsorption during TiO_2 ALD (RBS and SEM). On the other hand, when DMA-TMS is used as the SMI, we observe fewer TiO_2 nanoparticles as compared to the HMDS passivated surface (Fig. 4c). After 300 cycles on the DMA-TMS passivated surface, the particles have become larger and start to coalesce (Fig. 4d). The existence of nanoparticles and islands of different sizes has been explained by continuous regeneration of nucleation sites during the ALD process, resulting in islands of different sizes.[38] More extensive studies are required to determine a growth model that can describe the TiO_2 ALD on SiO_2 passivated with the different SMIs.

ACCEPTED MANUSCRIPT
Journal of Vacuum Science & Technology A
This is the author's peer reviewed, accepted manuscript. However, the online version of record will be different from this version once it has been copyedited and typeset.
PLEASE CITE THIS ARTICLE AS DOI: 10.1116/6.0002347

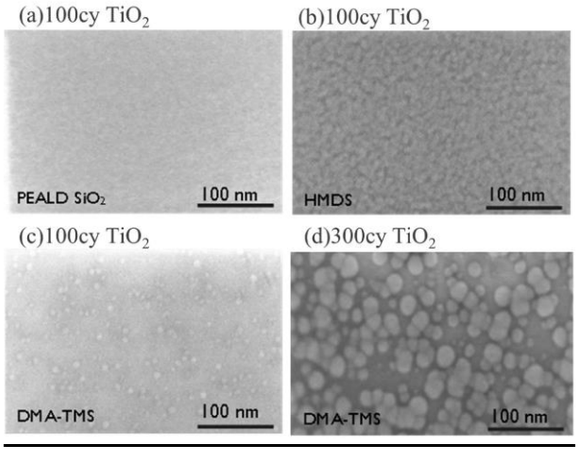

FIG. 4. SEM images of TiO_2 ALD (150 °C) (a) 100cy on untreated SiO_2 (b) 100cy on HMDS (300 s, 135 °C) treated SiO_2 (c) 100cy and (d) 300cy on DMA-TMS (300 s, 250 °C) treated SiO_2, indicating different growth modes.

Studying the temperature dependence of selectivity can provide understanding on the mechanism behind selectivity loss. We therefore explore the DMA-TMS passivation (250 °C, 300 s) in combination with additional ALD materials and temperatures. We evaluate the selectivity during TiO_2 ($TiCl_4/H_2O$) and TiN ($TiCl_4/NH_3$) ALD at deposition temperatures between 125 and 390 °C by RBS. The selectivity (relative to the untreated SiO_2 growth surface) is plotted as a function of film thickness on the growth surface in Fig. 5. The optimal temperature window for ASD of TiO_2 is between 125 and 150 °C. Higher deposition temperatures cause faster selectivity loss as a function of thickness. This is attributed to the reaction of TMS surface groups with the $TiCl_4$ precursor that occur more quickly at higher deposition temperatures. For the lower deposition temperatures, unwanted physisorption of precursors on the non-growth surface could cause selectivity loss and extended purging may improve selectivity.[25,39] For TiN, the highest selectivity is also achieved at the lowest temperature (300 °C), resulting in S = 1 after ~3 nm deposition on SiO_2. Increasing the TiN ALD temperature negatively impacts selectivity, presumably due to reaction of $TiCl_4$ with TMS surface groups. At the same temperature, the $TiCl_4/NH_3$ process is more selective

ACCEPTED MANUSCRIPT
Journal of Vacuum Science & Technology A
This is the author's peer reviewed, accepted manuscript. However, the online version of record will be different from this version once it has been copyedited and typeset.
PLEASE CITE THIS ARTICLE AS DOI: 10.1116/6.0002347

compared to the $TiCl_4/H_2O$ process. This has previously been linked to the lower partial pressure of the $TiCl_4$ precursor (0.5 Torr vs 2 Torr respectively) during the process rather than the impact of the coreagent.[25,40] Thus, the optimal conditions for selectivity may also depend on the precursor doses used in the ALD process.

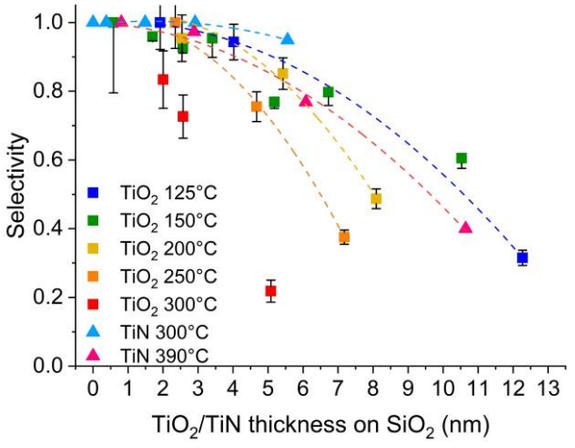

FIG. 5. Effect of ALD temperature on selectivity for TiO_2 ($TiCl_4/H_2O$) and TiN ($TiCl_4/NH_3$) ALD, with untreated SiO_2 as growth surface and DMA-TMS (250 °C, 300 s) treated SiO_2 as non-growth surface. The dashed lines are provided as guide to the eye. The reported error bars on the selectivity are determined through error propagation based on the uncertainties of the RBS measurements (experimental details).

C. DMA-TMS reaction on metal oxide substrates

To achieve AS-ALD, the SMI not only needs to react on the non-growth surface area where it blocks adsorption during subsequent ALD, it also needs to be unreactive towards the growth surface area where adsorption and growth are desired during ALD. In this section, we therefore investigate the reactivity of DMA-TMS with a range of substrates. We focus on the DMA-TMS treatment at 250 °C as the previous section indicated fast reaction on hydroxylated SiO_2 and most effective inhibition during ALD. To seek insight in how surface properties affect reactivity towards DMA-TMS, we consider a broad range of materials, namely MgO, HfO_2, ZrO_2, Al_2O_3, TiO_2 (TiN/TiO_x), SiO_2, SnO_2, $SnO_xC_yH_z$, MoO_x, and WO_3, with their surface properties summarized in Table 1. The analysis of the acidic and basic properties of substrates

ACCEPTED MANUSCRIPT
Journal of Vacuum Science & Technology A
This is the author's peer reviewed, accepted manuscript. However, the online version of record will be different from this version once it has been copyedited and typeset.
PLEASE CITE THIS ARTICLE AS DOI: 10.1116/6.0002347

and SMI could provide understanding to possibly predict compatibility of substrates and SMIs.[18] The basic amide ligands of aminosilane inhibitors react with the acidic hydroxyl groups on SiO_2 surfaces.[18] The interaction can depend on the polarity of the metal(loid)-oxygen and oxygen-hydrogen bonds and on the surface acidity. To systematically analyze the potential impact of surface acidity, we calculate the surface acidity from the Sanderson electronegativity (EN).[18,46] The values are listed in Table 1, together with the metal(loid) electronegativity (EN). The materials cover a broad acidity range, with surfaces that are less acidic (MgO, HfO_2, ZrO_2, Al_2O_3, TiO_2 (TiN/TiO_x)), similarly acidic (SnO_2) and more acidic (MoO_x, WO_3) as compared to SiO_2 (Table 1). The surface roughness and phase of the materials is also shown in Table 1. As the OH density is not known for the surfaces considered here (except SiO_2), and may vary for the different surfaces, we cannot investigate the impact of OH density in the current study. The metal(loid) ionic radius is given to possibly account for steric considerations in H-bonding. Each surface is characterized with WCA and XPS measurements before and after DMA-TMS treatment, with results shown in Fig. 6 and Table 1.

Interestingly, DMA-TMS does not form a dense TMS-layer on any of the surfaces considered here. This is indicated by the low WCA values which remain below 50° after DMA-TMS exposure (Fig. 6, Table 1). Small differences can be observed for the different metal oxide surfaces. MgO and WO_3 are the least reactive, as the WCA values do not change for DMA-TMS treatment times up to 1800 s (Fig. 6a, b). We see a slight increase in WCA value for MoO_x, HfO_2, Al_2O_3, ZrO_2, SnO_2 and $SnO_xC_yH_z$ ($x>1$) substrates. In contrast, we see a slight decrease in WCA for the TiO_x substrate, as the initial WCA value is higher compared to other surfaces. The negligible to small changes in WCA values indicate that either few TMS groups exist, or that other surface reactions occur that introduce surface species other than TMS groups.

ACCEPTED MANUSCRIPT
Journal of Vacuum Science & Technology A
This is the author's peer reviewed, accepted manuscript. However, the online version of record will be different from this version once it has been copyedited and typeset.
PLEASE CITE THIS ARTICLE AS DOI: 10.1116/6.0002347

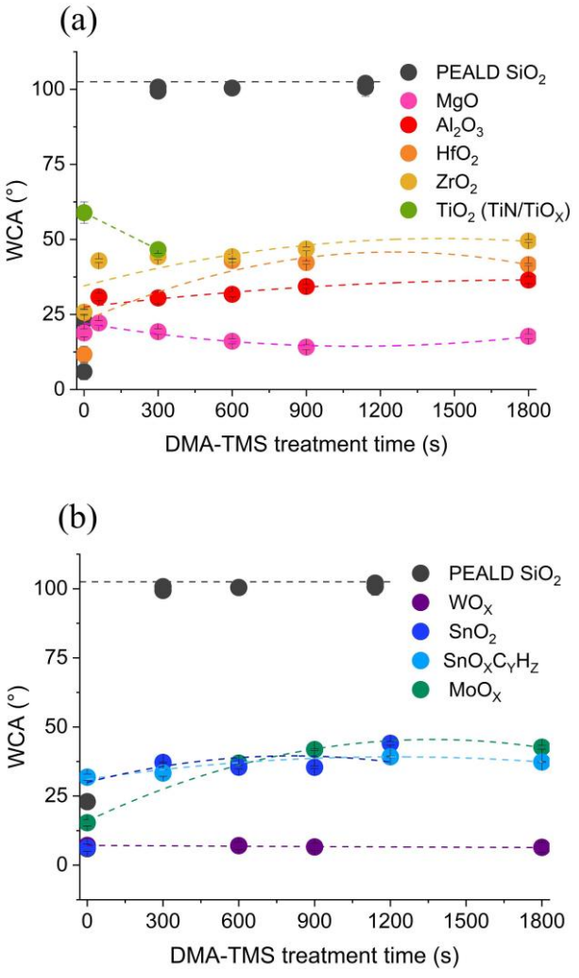

FIG. 6. (a) Effect of DMA-TMS treatment (250 °C) on the WCA of MgO, Al_2O_3, HfO_2, ZrO_2 and TiO_2 (TiN/TiOx). (b) Effect of DMA-TMS treatment (250 °C) on the WCA of WO_3, SnO_2, $SnO_xC_yH_z$ and MoO_x. Data for DMA-TMS passivation on PEALD SiO_2 is included for comparison. The dashed lines are provided as guide to the eye.

ACCEPTED MANUSCRIPT
Journal of Vacuum Science & Technology A
This is the author's peer reviewed, accepted manuscript. However, the online version of record will be different from this version once it has been copyedited and typeset.
PLEASE CITE THIS ARTICLE AS DOI: 10.1116/6.0002347

TABLE 1. Summary of the results for DMA-TMS reaction with different substrates: DMA-TMS reaction time, initial WCA before DMA-TMS reaction, WCA for saturated DMA-TMS reaction, and change in WCA value upon DMA-TMS reaction, XPS Si2p binding energy, XPS chemical composition of the Si surface species, XPS Si-content (all for XPS take-off angle (TOA) of 20°), Sanderson electronegativity of metal(loid) ion (S_M) [42–46], ionic radius of metal(loid) (R) [47], calculated surface acidity (SA),[18,46] AFM roughness and phase of the initial surfaces. The Sanderson electronegativity for oxygen (S_O) is 3.65 [43,45]. *Data Job Soethoudt et al.[25]

	DMA-TMS time (s)	WCA (°)			Si2p BE (eV)	Si species (x>1)	Si content (at/nm²)		R (pm)	S_M	SA	Rms roughness (nm)	Phase
		initial	saturation	Δ			300s DMA-TMS	1800s DMA-TMS					
MgO	1800	19	18	1	101-102.5	$OSi(CH_3)_3$, $SiO_xC_yH_z$	noise	~0.5	72	1.32	0.46	0.76	amorphous, nanocrystalline
HfO_2	1800	12	42	30	101-102.5	$OSi(CH_3)_3$, $SiO_xC_yH_z$	~0.9	/	71	0.81	0.9	0.57	nanocrystalline
ZrO_2	1800	26	50	24	101-102.5	$OSi(CH_3)_3$, $SiO_xC_yH_z$	~1.5	~0.8	72	0.9	1.07	0.55	nanocrystalline
Al_2O_3	1800	26	36	10	101.5	$OSi(CH_3)_3$, $SiO_xC_yH_z$	~0.5	~0.7	54	1.71	1.47	0.23	amorphous
TiO_2 (TiN/TiO_x)	300	59	47	14	101	$OSi(CH_3)_3$, $SiO_xC_yH_z$	~0.1	/	67	1.5	2	1.1	amorphous
SiO_2	300	6	101	95	101	$OSi(CH_3)_3$	~2.0	/	40	2.14	2.73	0.14	amorphous
SnO_2	900	6	44	38	101	$OSi(CH_3)_3$	/	/	69	2.3	2.88	0.45	amorphous, nanocrystalline
$SnO_xC_yH_z$	1800	32	37	5	101	$OSi(CH_3)_3$	/	/	69	/	/	0.22	amorphous
Ru/RuO_x*	300	/	/	/	102.5	$SiO_xC_yH_z$	< 2	/	68	/	/	/	amorphous
Mo/MoO_x	1800	34	38	4	102.5	$SiO_xC_yH_z$	~1.8	/	65	1.73	3.12	0.34	amorphous
W/WO_3	1800	7	6	1	102.5	$SiO_xC_yH_z$	~0.5	/	66	1.67	3.91	0.28	amorphous

XPS is used to further analyze potential chemical changes in surface composition. As explained above, the presence of TMS surface groups should be indicated in the Si2p spectrum at a binding energy of 101-101.5 eV. [7,25] Surface species with Si in a higher oxidation state, for example $SiO_xC_yH_z$ with x>1, should appear at a higher binding energy.[25,41] Such species have been formed during DMA-TMS reaction on Ru/RuO_x substrates.[25] The estimated Si-content and the XPS Si2p binding energy for DMA-TMS reaction on the different substrates are

ACCEPTED MANUSCRIPT
Journal of Vacuum Science & Technology A
This is the author's peer reviewed, accepted manuscript. However, the online version of record will be different from this version once it has been copyedited and typeset.
PLEASE CITE THIS ARTICLE AS DOI: 10.1116/6.0002347

summarized in Table 1, together with the change in WCA. All XPS spectra are reported and described in supplementary material at [URL will be inserted by AIP Publishing] (Fig. S1 – S5).

The results first show that the presence of TMS groups has a larger impact on the WCA change than $SiO_xC_yH_z$ (x>1) surface species: a small amount of TMS groups result in a larger increase in the WCA value as compared to a larger amount of $SiO_xC_yH_z$ (x>1) surface species (Table 1). Indeed, TMS surface species contain more alkyl ligands as compared to $SiO_xC_yH_z$ (x>1) suboxide species, and therefore have a more hydrophobic character.

We can now investigate the extent to which surface acidity affects the DMA-TMS reaction. Metal oxide surfaces with a lower surface acidity than SiO_2, namely HfO_2, Al_2O_3, ZrO_2, TiO_2 and MgO, have a more alkaline surface character as compared to SiO_2. The interaction of DMA-TMS with these surfaces is indeed weaker, as indicated by the lower TMS surface concentrations and the much smaller changes in WCA (Table 1). The oxidation state of Si is not much affected by reaction with these metal oxide surfaces, as the surface species are mainly TMS groups with only minor contributions from $SiO_xC_yH_z$ (x>1) surface species. The DMA-TMS reaction on TiN with native TiO_2 results in only 5% TMS coverage, as estimated by XPS,[7,25] presumably because DMA-TMS reacts only with isolated Ti-OH surface groups and not with Ti-O-Ti or H-bonded Ti-OH surface groups.[25]

In contrast, the surfaces with a higher surface acidity than SiO_2 do not interact more with DMA-TMS, contrary to what would be expected purely based on the surface acidity (Table 1). Moreover, the extents and types of reactions depend on the metal oxide, indicating that surface acidity is not the only factor that affects the substrate-inhibitor interaction. The MoO_x, RuO_x and WO_3 surfaces oxidize DMA-TMS as $SiO_xC_yH_z$ surface species are observed in the Si2p spectrum while no TMS species are visible. The obtained Si content becomes ~1.8 Si/nm^2 after 300 s DMA-TMS reaction on the Mo/MoO_x surface (Fig. S3). The surface

ACCEPTED MANUSCRIPT
Journal of Vacuum Science & Technology A
This is the author's peer reviewed, accepted manuscript. However, the online version of record will be different from this version once it has been copyedited and typeset.
PLEASE CITE THIS ARTICLE AS DOI: 10.1116/6.0002347

composition is therefore similar to that for DMA-TMS reaction on Ru/RuO_x, where it was demonstrated that DMA-TMS reduces reactive O sites at the Ru surface enabling the formation of $SiO_xC_yH_z$ islands.[25] Indeed, the Mo3d spectrum shows a decrease in the $Mo\text{-}O_X$ content after 1800 s DMA-TMS treatment, in line with this reaction (Fig. S3b). While the Si content is similar as for the dense TMS layer formed on SiO_2, the morphology is quite different. The $SiO_xC_yH_z$ deposition has been shown to be island-like for DMA-TMS reaction on the RuO_x surface, leaving most of the Ru surface available and reactive for ALD.[25] We could detect only a very small amount of Si surface species for 300 s DMA-TMS reaction on WO_3 (~0.5 Si/nm^2) and the spectrum is noisy (Fig. S4a). This is consistent with the small changes in WCA upon DMA-TMS reaction (0.7°). Similar as for MoO_x and RuO_x, the W4f spectrum showed WO_3 reduction after 1800 s DMA-TMS treatment (Fig. S4b).

SnO_2 and SiO_2 have a similar surface acidity (2.88 and 2.73 for SnO_2 and SiO_2, respectively). Nevertheless, the change in WCA upon DMA-TMS reaction is smaller for SnO_2 as compared to SiO_2, indicating a much lower TMS surface concentration in line with the XPS spectra. MgO and WO_3, with the lowest and highest surface acidity respectively, are the least reactive towards DMA-TMS. The lower reactivity of SnO_2 towards DMA-TMS could be due to a lower concentration of surface OH groups, and/or a lower concentration of isolated OH groups versus H-bonded OH groups. This could be in line with the larger ionic radius of Sn.

Another factor that could affect surface reactivity is surface roughness. The surfaces considered here contain various degrees of surface roughness. No clear correlation between surface roughness and the changes in surface composition upon DMA-TMS reaction appears from Table 1. The two smoothest surfaces are SiO_2 and Al_2O_3 and those two surfaces show markedly different reactivity. We conclude that the reactivity most likely results from a complex interplay of different factors that can include surface acidity, OH density, H-bonding, roughness, phase, stoichiometry and catalytic properties.

ACCEPTED MANUSCRIPT
Journal of Vacuum Science & Technology A
This is the author's peer reviewed, accepted manuscript. However, the online version of record will be different from this version once it has been copyedited and typeset.
PLEASE CITE THIS ARTICLE AS DOI: 10.1116/6.0002347

Finally, we investigate the impact of organic surface groups by comparing the DMA-TMS reaction for the SnO_2 and $SnO_xC_yH_z$ (x>1) substrates. The $SnO_xC_yH_z$ (x>1) surface contains organic ligands, as the initial WCA (33.7°) is higher compared to that for SnO_2 (6.3°). The concentration of TMS groups on $SnO_xC_yH_z$ (x>1) surface after DMA-TMS reaction is lower as compared to the DMA-TMS treated SnO_2 surface, as indicated by the smaller shoulder in the Si2p spectra (Fig. S5). This is in accordance with the smaller change in WCA (ΔWCA = 5.5°). The lower reactivity of the $SnO_xC_yH_z$ (x>1) surface compared to SnO_2 may be related to the lower initial content of surface OH groups on the $SnO_xC_yH_z$ (x>1) surface. Furthermore, the organic ligands may hinder the reaction of DMA-TMS with the surface OH groups.

To conclude, DMA-TMS does not form a dense TMS-layer on any of the metal oxide surfaces considered here, indicating that they could all act as growth surfaces during area-selective deposition. Materials with lower, similar, and higher Sanderson surface acidity than SiO_2 show less reaction with DMA-TMS, suggesting that surface acidity is not the only factor affecting the substrate-inhibitor interaction. TMS and/or $SiO_xC_yH_z$ surface species can occur in low concentrations and, as such may affect the interface composition and structure.

D. Effect of DMA-TMS treatment on ALD growth on metal oxides substrates

To verify if the metal oxide surfaces can indeed function as growth surfaces during AS-ALD, we investigate TiO_2 or TiN ALD on selected surfaces after DMA-TMS treatment. We study TiO_2 growth with the $TiCl_4/H_2O$ ALD process at 150 °C on three representative metal oxide substrates, namely HfO_2, Al_2O_3 and MoO_x. We study the ALD growth evolution using RBS on the untreated and DMA-TMS treated substrates and compare the growth evolution to that for untreated and DMA-TMS treated SiO_2. Results are shown in Fig. 7.

ACCEPTED MANUSCRIPT
Journal of Vacuum Science & Technology A
This is the author's peer reviewed, accepted manuscript. However, the online version of record will be different from this version once it has been copyedited and typeset.
PLEASE CITE THIS ARTICLE AS DOI: 10.1116/6.0002347

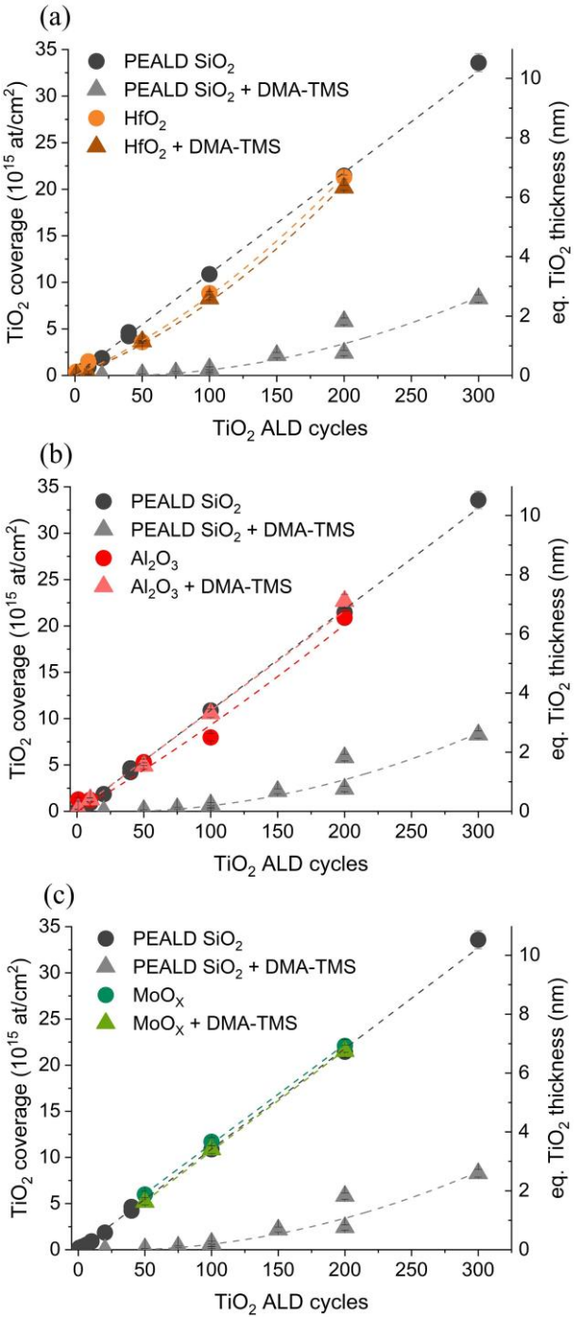

FIG. 7. TiO_2 growth ($TiCl_4/H_2O$ ALD, 150 °C) on (a) HfO_2, (b) Al_2O_3 and (c) MoO_x before and after DMA-TMS treatment (300 s, 250 °C) compared to the linear growth on untreated SiO_2 and the delayed growth on DMA-TMS passivated SiO_2. The dashed lines are provided as guide to the eye. The reported error bars on the TiO_2 coverage reflect the uncertainties of the RBS measurements (experimental details).

TiO_2 growth curves are linear on the untreated and DMA-TMS treated metal oxide substrates (Fig. 7). No TiO_2 growth delay is observed on DMA-TMS treated HfO_2, Al_2O_3, or

ACCEPTED MANUSCRIPT
Journal of Vacuum Science & Technology A
This is the author's peer reviewed, accepted manuscript. However, the online version of record will be different from this version once it has been copyedited and typeset.
PLEASE CITE THIS ARTICLE AS DOI: 10.1116/6.0002347

MoO_x, unlike on DMA-TMS treated SiO_2. This demonstrates that the concentrations of TMS or $SiO_xC_yH_z$ surface species on the metal oxide surfaces are sufficiently low to not inhibit TiO_2 ALD. This insight allows us to design ASD schemes with TMS passivated SiO_2 as the non-growth areas and the metal oxide substrates as potential growth areas.

We additionally study TiN ALD using $TiCl_4/NH_3$ at 390 °C on SnO_2 and $SnO_xC_yH_z$ (x>1) substrates before and after DMA-TMS treatment, with results shown in Fig. 8. For TiN ALD on the untreated SnO_2, the intercept of the growth curve is zero, indicating that TiN growth occurs readily (Fig. 8a). For TiN ALD on the DMA-TMS treated SnO_2, we observe a slightly positive intercept on the X-axis, indicating a minor growth delay of about 25 ALD cycles. This means that the initial growth rate is slightly enhanced on untreated SnO_2 compared to untreated SiO_2. After 50 cycles, the growth rate on the untreated and DMA-TMS treated substrate is similar. The moderate concentration of TMS groups on the DMA-TMS treated SnO_2 substrate (WCA and XPS) seems to at least partially block adsorption of the ALD precursors on SnO_2 reactive sites, although not to the same extent as observed on DMA-TMS treated SiO_2 (i.e. ~100 cycles growth delay). An XPS depth profile can be found in the supplementary material at [URL will be inserted by AIP Publishing], after TiN ALD confirms the presence of Ti and N on top of the SnO_2 film (Fig. S6). For $SnO_xC_yH_z$ (x>1), the growth behavior is not affected by DMATMS reaction (Fig. 8b). The initial growth on $SnO_xC_yH_z$ (x>1) is enhanced in the first 100 cycles compared to SiO_2, which is investigated further below. Thus, as expected, the low TMS concentrations (WCA, XPS) do not inhibit TiN ALD on SnO_2 and $SnO_xC_yH_z$ (x>1), while for the DMA-TMS passivated SiO_2 TiN growth is delayed for ~100 ALD cycles.

ACCEPTED MANUSCRIPT
Journal of Vacuum Science & Technology A
This is the author's peer reviewed, accepted manuscript. However, the online version of record will be different from this version once it has been copyedited and typeset.
PLEASE CITE THIS ARTICLE AS DOI: 10.1116/6.0002347

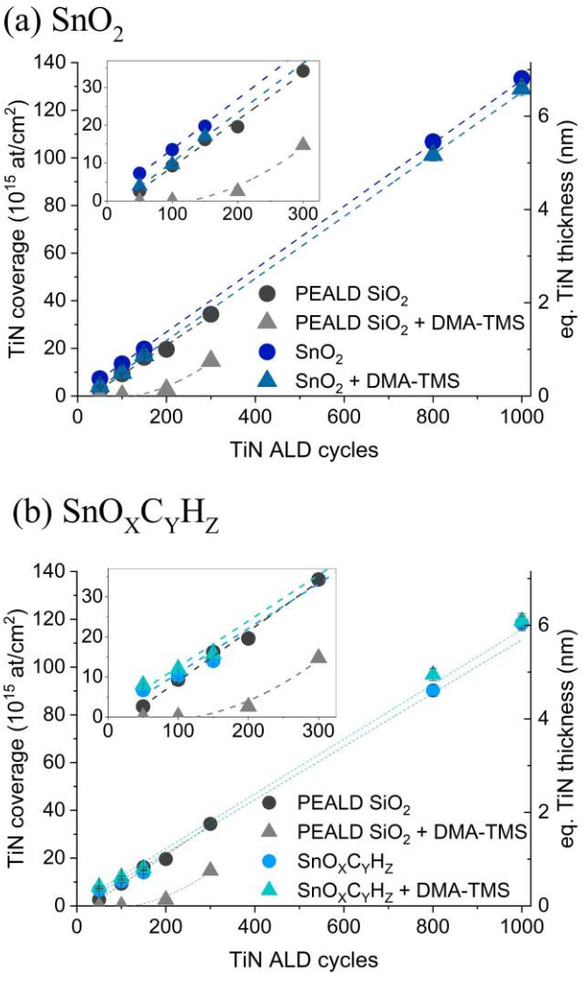

FIG. 8. (a) TiN growth ($TiCl_4/NH_3$ ALD, 390 °C) on untreated and DMA-TMS (300 s, 250 °C) treated SnO_2 and SiO_2. (b) TiN growth ($TiCl_4/NH_3$ ALD, 390 °C) on untreated and DMA-TMS (300 s, 250 °C) treated $SnO_xC_yH_z$ (x>1) and SiO_2. The dashed lines are provided as guide to the eye.

To understand the initial higher growth rate of TiN on DMA-TMS passivated $SnO_xC_yH_z$ (x>1), TEM images were taken after 1000 cycles of TiN ALD on DMA-TMS treated and untreated $SnO_xC_yH_z$ (x>1) to visualize the Ti spatial distribution, with images shown in Fig. 9. The TEM images indicate the presence of a mixed layer of $SnO_xC_yH_z$ (x>1) and TiN (Fig. 9a, c). TEM/EDS gives a more detailed look at the composition of this layer (Fig. 9 a,b). For TiN ALD on the DMA-TMS treated $SnO_xC_yH_z$ (x>1) surface, three layers can be distinguished: at the bottom, a fully mixed $SnO_xC_yH_z$ (x>1)/TiN layer of ~6.4 nm is observed, which transitions

ACCEPTED MANUSCRIPT
Journal of Vacuum Science & Technology A
This is the author's peer reviewed, accepted manuscript. However, the online version of record will be different from this version once it has been copyedited and typeset.
PLEASE CITE THIS ARTICLE AS DOI: 10.1116/6.0002347

through an intermediate layer of ~1.8 nm (middle layer) to a pure TiN layer of ~29.6 nm (top layer, Fig. 9a). The sum of the mixed and intermediate layer thicknesses (i.e., 8.2 nm) is about the thickness of the initial $SnO_xC_yH_z$ (x>1) layer (8.9 nm). For TiN ALD on the untreated $SnO_xC_yH_z$ (x>1) layer, we can distinguish two layers: a $SnO_xC_yH_z$ (x>1)/TiN mixed layer (~7.1 nm) and pure TiN layer (~31.5 nm) (Fig. 9b). No transition layer is visible within the resolution of the TEM measurement. These images indicate diffusion and reaction of the precursors into the bulk of the Sn-based material. EDS analysis confirms that the bottom layer contains both Sn and Ti, but very little N is present (Fig. 9c,d).

ACCEPTED MANUSCRIPT
Journal of Vacuum Science & Technology A
This is the author's peer reviewed, accepted manuscript. However, the online version of record will be different from this version once it has been copyedited and typeset.
PLEASE CITE THIS ARTICLE AS DOI: 10.1116/6.0002347

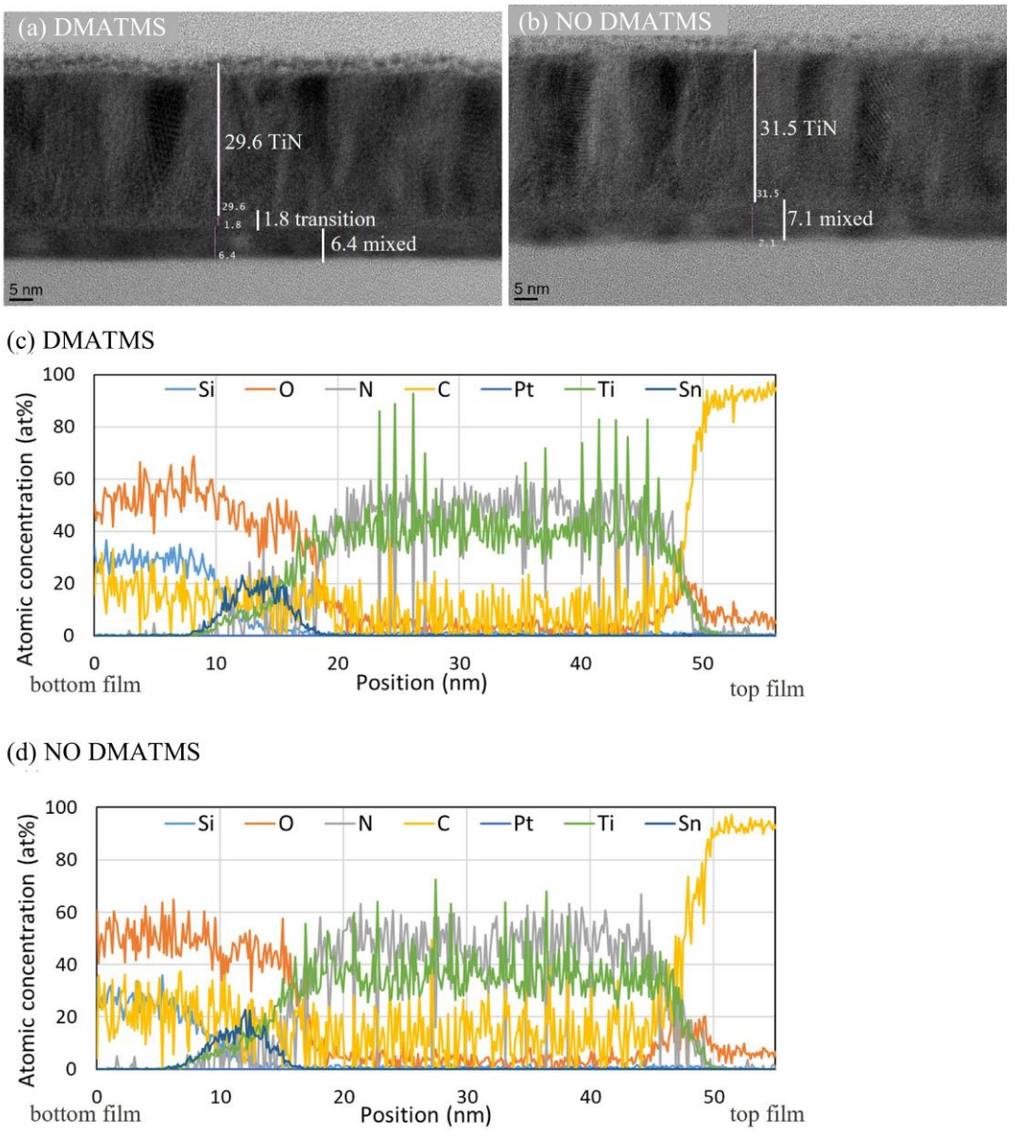

FIG. 9. TEM images (a)/(c) and EDS linescans (b)/(d) for 1000 cycles TiN ALD on DMA-TMS treated and untreated $SnO_xC_yH_z$ (x>1), respectively, to visualize the Ti distribution.

To further elucidate the interactions between TiN precursors and the $SnO_xC_yH_z$ (x>1) layer, we perform RBS analysis after 1 and 10 pulses of the $TiCl_4$ and NH_3 precursors seperately on $SnO_xC_yH_z$ (x>1) (Fig. 10a, no DMA-TMS treatment). These results indicate a decrease in Sn areal density of $6*10^{15}$ at/cm^2 and an increase in Ti areal density of $4.5*10^{15}$ at/cm^2 between the 1st and 10th dose. The $TiCl_4$ reaction is not saturated in this case, since after 10 pulses the Ti concentration surpasses the monolayer content. On the other hand, no change

ACCEPTED MANUSCRIPT
Journal of Vacuum Science & Technology A
This is the author's peer reviewed, accepted manuscript. However, the online version of record will be different from this version once it has been copyedited and typeset.
PLEASE CITE THIS ARTICLE AS DOI: 10.1116/6.0002347

in Sn areal density can be seen after NH_3 pulsing under the same conditions. This means that Sn is not removed due to the impact of the temperature or NH_3, but most likely due to a ligand exchange reaction between the $TiCl_4$ precursor and Sn-O. This explains the presence of Ti but very little N in the intermixed layer (Fig. 9 c,d). Although the reaction of $TiCl_4$ with OH sites is thermodynamically more favoured (bond dissociation enthalpy: 83 kJ/mol for SnO, 260 kJ/mol for OH[48]), the reaction of $TiCl_4$ with Sn-O sites might happen due to a very low OH concentration. A possible hypothesis is that $TiCl_4$ binds to O in the film, and Cl ligands of the $TiCl_4$ react with Sn during the initial cycles and volatile $SnCl_4$ is formed:

$$SnO_XC_YH_Z \quad + M\ TiCl_4 \rightarrow Sn_{1-M}Ti_MO_XC_YH_Z \quad + M\ SnCl_4.$$

This leaves no Cl ligands on Ti for the NH_3 precursor to react. Some of the Sn in the film is probably not accessible for reaction with $TiCl_4$, resulting in the $SnO_xC_yH_z$ (x>1)/Ti mixed layer. The intermediate layer could be formed due to a drop in Sn concentration after a certain amount has been replaced with Ti, initiating further growth through the $TiCl_4/NH_3$ ALD reaction on exposed Ti-Cl bonds.

Contrarily, the $TiCl_4$ precursor reaction on SnO_2 showed an increase in the Ti content of only 50% after 10 pulses while on $SnO_xC_yH_z$ (x>1) it increases with more than 400%. This indicates that the $TiCl_4$ probably reacts predominantly with Sn-O-H surface sites on SnO_2 and does not significantly react deeper in the film, probably due to the denser nature of the film compared to $SnO_xC_yH_z$ (x>1). In addition, it indicates that the reaction of $TiCl_4$ with SnO_2 is self-limiting and will saturate at the monolayer concentration. Understanding whether infiltration of Ti into the Sn-material occurs is important for the design of ASD schemes. In addition, the enhanced initial growth on the Sn-materials can be benificial for an ASD process with the Sn-substrates as the growth substrate.

ACCEPTED MANUSCRIPT
Journal of Vacuum Science & Technology A
This is the author's peer reviewed, accepted manuscript. However, the online version of record will be different from this version once it has been copyedited and typeset.
PLEASE CITE THIS ARTICLE AS DOI: 10.1116/6.0002347

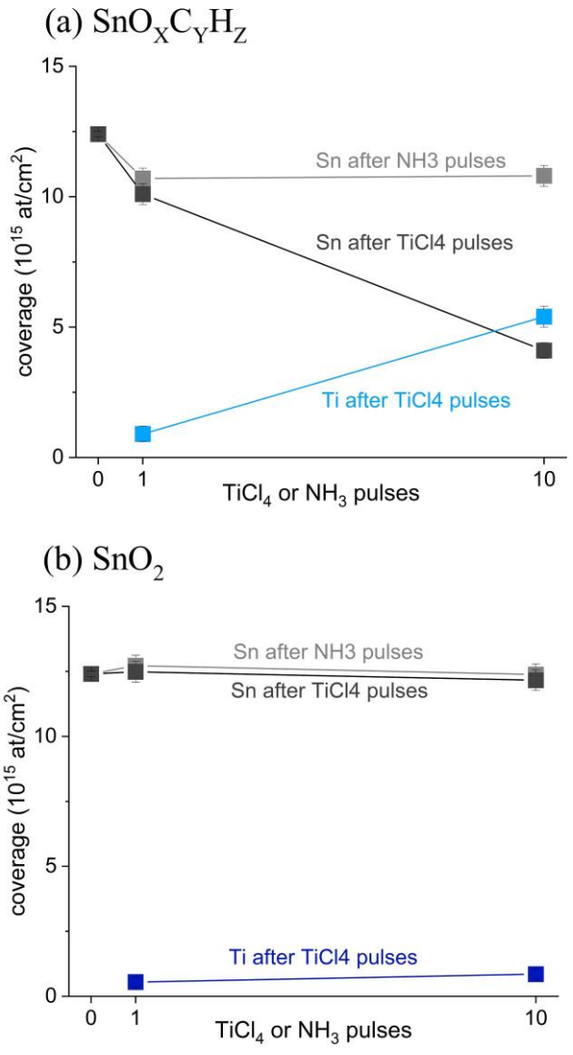

FIG. 10. Ti and Sn areal density after 0, 1 and 10 pulses of the $TiCl_4$ and NH_3 precursor on (a) $SnO_xC_yH_z$ (x>1) and (b) SnO_2. The Ti content does not saturate at monolayer level on $SnO_xC_yH_z$ (x>1), indicating infiltration and reaction in the bulk. The solid lines are provided as guide to the eye.

IV. CONCLUSIONS

This work provides insight into the reactions of aminosilane SMIs with various oxide surfaces. We demonstrate that DMA-TMS is more effective for SiO_2 passivation as compared to HMDS, as the DMA-TMS reaction saturates faster and results in a higher TMS surface concentration. Our insights suggest that DMA-TMS can be used in ASD processes to selectively passivate SiO_2 with respect to MoO_x, WO_3, RuO_x, HfO_2, Al_2O_3, ZrO_2, TiO_2

ACCEPTED MANUSCRIPT
Journal of Vacuum Science & Technology A
This is the author's peer reviewed, accepted manuscript. However, the online version of record will be different from this version once it has been copyedited and typeset.
PLEASE CITE THIS ARTICLE AS DOI: 10.1116/6.0002347

(TiN/TiO_x), MgO and SnO_2 substrates, as those surfaces remain reactive for ALD while SiO_2 is passivated. Moreover, each of the investigated metal oxide substrates could be used in a cyclic DMA-TMS passivation/deposition/etch ASD process, to improve the thickness of the selectively grown layer on SiO_2 and should be the subject of future work. As such, the knowledge obtained in this study can be implemented to design AS-ALD strategies using SMIs to improve selectivity in advanced technology nodes.

We observed a different reactivity for SnO_2 and $SnO_xC_yH_z$ substrates and demonstrated that both bulk composition and surface stoichiometry affect the adsorption of DMATMS. This provides an interesting outlook for future investigations of ASD for patterning applications, that could focus on selectivity tuning by the surface and/or bulk stoichiometry of the $SnO_xC_yH_z$ EUV resist materials.

We demonstrate that factors such as surface acidity and composition are some of several factors that affect the reactivity towards aminosilanes and the resulting Si-species at the surface. More extensive studies are needed to ultimately enable predictions of the compatibility of substrates and SMIs. The reaction mechanisms and formed surface structures could be explored in more detail by in-situ analysis to fully understand the relation and the impact of other factors, including OH density, H-bonding, phase, catalytic properties, and surface roughness.

ALD conditions and precursors ($TiCl_4$, H_2O, NH_3) strongly affect the selectivity, thus, tuning these can further improve selectivity. We demonstrated that DMA-TMS forms residual TMS and/or $SiO_xC_yH_z$ surface species that do not markedly inhibit ALD. The potential impact of surface poisoning on selectivity loss and interfacial $SiO_xC_yH_z$ ($x>1$) species merits further investigation. In addition, this paper considered blanket surfaces. Future research should seek to extend these results to patterned substrates.

ACCEPTED MANUSCRIPT
Journal of Vacuum Science & Technology A
This is the author's peer reviewed, accepted manuscript. However, the online version of record will be different from this version once it has been copyedited and typeset.
PLEASE CITE THIS ARTICLE AS DOI: 10.1116/6.0002347

SUPPLEMENTAL INFORMATION

See supplementary material at [URL will be inserted by AIP Publishing] for additional XPS spectra and depth profiles.

ACKNOWLEDGEMENTS

The authors acknowledge Inpria Corporation for providing the metal-oxide resist and Peter De Schepper and Sonia Castellanos Ortega from Inpria Corporation for valuable discussions. The authors acknowledge Ilse Hoflijk, Anja Vanleenhove and Thierry Conard from imec for their discussions involving XPS characterization and data analysis. We thank Jorne Domen from KU Leuven for assistance in sample characterization. Jan-Willem Clerix acknowledges funding from The Research Foundation – Flanders (FWO) for a PhD fellowship strategic basic research (project number 1SB4321N).

AUTHOR DECLARATIONS

The authors have no conflicts to disclose.

DATA AVAILABILITY

The data that supports the findings of this study are available within the article and its supplementary material at [URL will be inserted by AIP Publishing].

FUNDING SOURCES

Jan-Willem Clerix acknowledges funding from The Research Foundation – Flanders (FWO) for a PhD fellowship strategic basic research (project number 1SB4321N).

REFERENCES

(1) G. N. Parsons and R. D. Clark, *Chem. Mater.* **32**, 4920 (2020). https://doi.org/10.1021/acs.chemmater.0c00722.
(2) R. Clark, K. Tapily, K. H. Yu, T. Hakamata, S. Consiglio, D. O'Meara, C. Wajda, J.

ACCEPTED MANUSCRIPT
Journal of Vacuum Science & Technology A
This is the author's peer reviewed, accepted manuscript. However, the online version of record will be different from this version once it has been copyedited and typeset.
PLEASE CITE THIS ARTICLE AS DOI: 10.1116/6.0002347

Smith, G. Leusink, *APL Mater.* **6**, 058203 (2018).
(3) A. J. M. Mackus, A. A. Bol, W. M. M. Kessels, *Nanoscale* **6**, 10941 (2014).
(4) A. J. M. Mackus, M. J. J. Merkx, W. M. M. Kessels, *Chem. Mater.* **31**, 2 (2019).
(5) S. K. Song, H. Saare, G. N. Parsons, *Chem. Mater.* **31**, 4793 (2019).
(6) S. E. Atanasov, B. Kalanyan, G. N. Parsons, *J. Vac. Sci. Technol. A* **34**, 01A148. (2016).
(7) J. Soethoudt, S. Crahaij, T. Conard, A. Delabie, *J. Mater. Chem. C* **7**, 11911 (2019).
(8) R. Wojtecki, M. Mettry, N. F. Fine Nathel, A. Friz, A. De Silva, N. Arellano, H. Shobha, *ACS Appl. Mater. Interfaces* **10**, 38630 (2018).
(9) F. Grillo, J. Soethoudt, E. A. Marques, L. de Martín, K. van Dongen, R. J. R. van Ommen, A. Delabie, *Chem. Mater.* **32**, 9560 (2020).
(10) K. Cao, J. Cai, R. Chen, *Chem. Mater. 32*, 2195 (2020).
(11) J. A. Singh, N. F. W. Thissen, W. H. Kim, H. Johnson, W. M. M. Kessels, A. A. Bol, S. F. Bent, A. J. M. Mackus, *Chem. Mater.* **30**, 663 (2018).
(12) E. Stevens, Y. Tomczak, B. T. Chan, E. Altamirano Sanchez, G. N. Parsons, A. Delabie, *Chem. Mater.* **30**, 3223 (2018).
(13) F. S. Minaye Hashemi, B. R. Birchansky, S. F. Bent, *ACS Appl. Mater. Interfaces*, **8**, 33264 (2016).
(14) F. S. M. Hashemi, S. F. Bent, *Adv. Mater. Interfaces* **3** 1600464 (2016).
(15) F. S. M. Hashemi, C. Prasittichai, S. F. Bent, *ACS Nano*, **9**, 8710 (2015).
(16) C. H. Chang, J.-D. Liao, J.-J. J. Chen, M.-S. Ju, C.-C. K. Lin, *Langmuir **20***, 11656 (2004).
(17) E. K. Seo, J. W. Lee, H. M. Sung-Suh, M. M. Sung, *Chem. Mater.* **16**, 1878 (2004).
(18) J. Yarbrough, A. B. Shearer, S. F. Bent, *J. Vac. Sci. Technol. A*, **39**, 021002 (2021).
(19) M. J. M. Merkx, A. Angelidis, A. Mameli, J. Li, P. C. Lemaire, K. Sharma, D. M. Hausmann, W. M. M. Kessels, T. E. Sandoval, A. J. M. Mackus, *J. Phys. Chem. C* **126**, 4845 (2021).
(20) D. Bobb-Semple, K. L. Nardi, N. Draeger, D. M. Hausmann, S. F. Bent, *Chem. Mater.* **31**, 1635 (2019).
(21) R. Chen, H. Kim, P. C. McIntyre, S. F. Bent, *Chem. Mater.* **17**, 536 (2005).
(22) L. Lecordier, S. Herregods, S. Armini, *J. Vac. Sci. Technol. A* **36**, 031605 (2018).
(23) T. Suh, Y. Yang, P. Zhao, K. U. Lao, H. Y. Ko, J. Wong, R. A. Distasio, J. R. Engstrom, *ACS Appl. Mater. Interfaces* **12**, 9989 (2020).
(24) R. Khan, B. Shong, B. G. Ko, J. K. Lee, H. Lee, J. Y. Park, I. K. Oh, S. S. Raya, H. M. Hong, K. B. Chung, E. J. Luber, Y. S. Kim, C. H. Lee, W. H. Kim, H. B. R. Lee, *Chem. Mater.* **30**, 7603 (2018).
(25) J. Soethoudt, Y. Tomczak, B. Meynaerts, B. T. Chan, A. Delabie, *J. Phys. Chem. C* **124**, 7163 (**2020**).
(26) W. Xu, P. C. Lemaire, K. Sharma, *J. Vac. Sci. Technol. A* **39**, 32402 (2021).
(27) Y. Au, Y. Lin, H. Kim, E. Beh, Y. Liu, R. G. Gordon, *J. Electrochem. Soc.* **157**, 6 D341 (2010).
(28) W. Xu, M. G. N. Haeve, P. C. Lemaire, K. Sharma, D. M. Hausmann, S. Agarwal, *Langmuir* **38**, 652 (2022).
(29) V. M. Gun'Ko, M. S. Vedamuthu, G. L. Henderson, J. P. Blitz, *J. Colloid Interface Sci.* **228**, 157 (2000).
(30) W. Hertl, M. L. Hair, *J. Phys. Chem.* **75**, 2181 (1971).
(31) W.-M. Yeh, D. E. Noga, R. A. Lawson, L. M. Tolbert, C. L. Henderson, *J. Chem. Phys.* **28**, 164106 (2010).
(32) R. A. Nye, K. van Dongen, H. Oka, D. De Simone, G. Parsons, A. Delabie, *Journal of Micro/Nanopatterning, Materials and Metrology* **21**, 041407 (2022).

ACCEPTED MANUSCRIPT
Journal of Vacuum Science & Technology A
This is the author's peer reviewed, accepted manuscript. However, the online version of record will be different from this version once it has been copyedited and typeset.
PLEASE CITE THIS ARTICLE AS DOI: 10.1116/6.0002347

(33) T. Imada, Y. Nakata, S. Ozaki, Y. Kobayashi, T. Nakamura, *Jpn. J. Appl. Phys.* **54**, 071502 (2015).
(34) L. L. Crowe, L. M. Tolbert, *Langmuir* **24**, 8541 (2008).
(35) L. Nyns, A. Delabie, M. Caymax, M. M. Heyns, S. Van Elshocht, C. Vinckier, S. De Gendt, *J. Electrochem. Soc.* **155**, G269 (2008).
(36) G. N. Parsons, *J. Vac. Sci. Technol. A* **37**, 020911 (2019).
(37) M. Junige, S. M. George, J. Vac. Sci. Technol. A 39, 023204 (2021).
(38) R. A. Nye, S. K. Song, K. Van Dongen, A. Delabie, G. N. Parsons, *Appl. Phys. Lett*. **121**, 082102 (2022).
(39) M. F. J. Vos, S. N. Chopra, M. A. Verheijen, J. G. Ekerdt, S. Agarwal, W. M. M. Kessels, A. J. M. Mackus, *Chem. Mater.* **31**, 3878 (2019).
(40) A. J. M. Mackus, M. A. Verheijen, N. Leick, A. A. Bol, W. M. M. Kessels, *Chem. Mater.* **25**, 1905 (2013).
(41) S. Jayachandran, A. Delabie, A. Billen, H. Dekkers, B. Douhard, T. Conard, J. Meersschaut, M. Caymax, W. Vandervorst, M. Heyns, *Appl. Surf. Sci.* **324**, 251 (2015).
(42) R. T. Sanderson, *J. Chem. Educ.* **48**, A561 (1971).
(43) R. T. Sanderson, *J. Am. Chem. Soc.* **105**, 2259 (1983).
(44) R. T. Sanderson, *Inorg. Chem.* **25**, 3518 (1986).
(45) R. T. Sanderson, *Inorg. Chem.* **25**, 1856 (1986).
(46) N. C. Jeong, J. S. Lee, E. L. Tae, Y. J. Lee, K. B. Yoon, *Angew. Chemie Int. Ed.* **47**, 10128 (2008).
(47) J. Halpern, U. Howard, https://chem.libretexts.org/@go/page/98634.
(48) Y. R. Luo, Comprehensive Handbook of Chemical Bond Energies (CRC Press, Boca Raton, 2007)

ACCEPTED MANUSCRIPT
Journal of Vacuum Science & Technology A
This is the author's peer reviewed, accepted manuscript. However, the online version of record will be different from this version once it has been copyedited and typeset.
PLEASE CITE THIS ARTICLE AS DOI: 10.1116/6.0002347

(a)

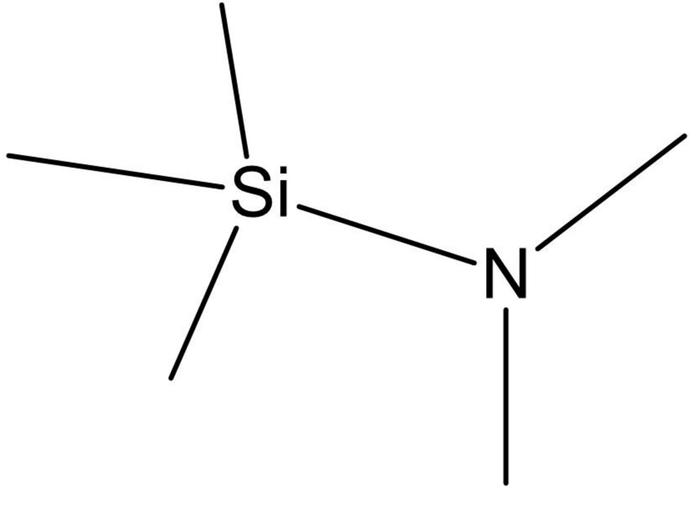

(b)

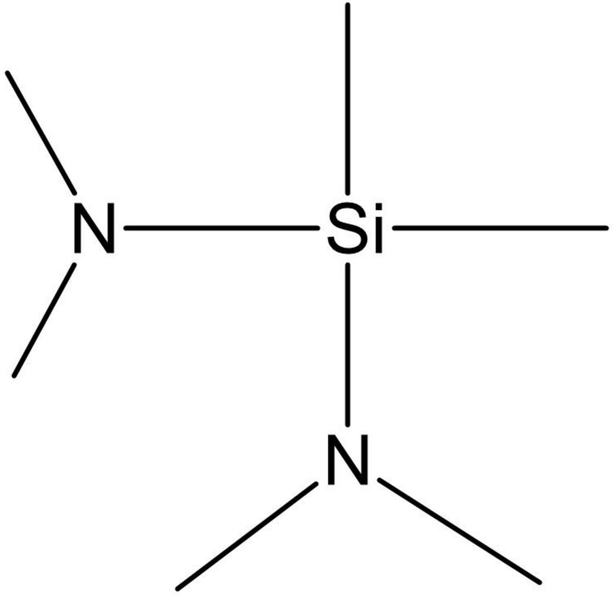

(c)

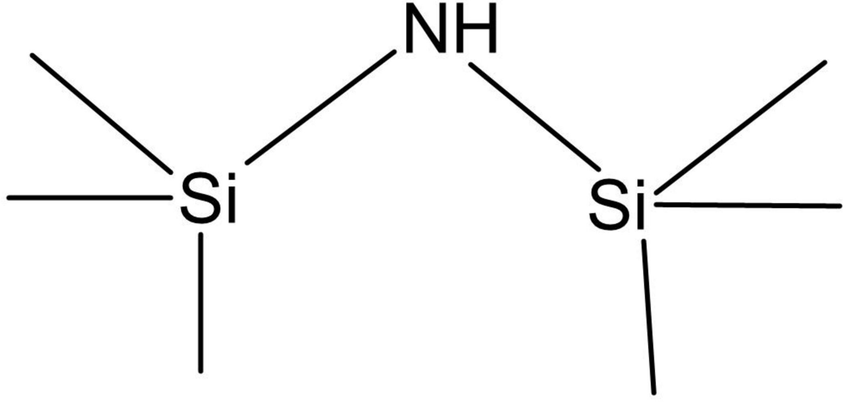

ACCEPTED MANUSCRIPT
Journal of Vacuum Science & Technology A

(a)

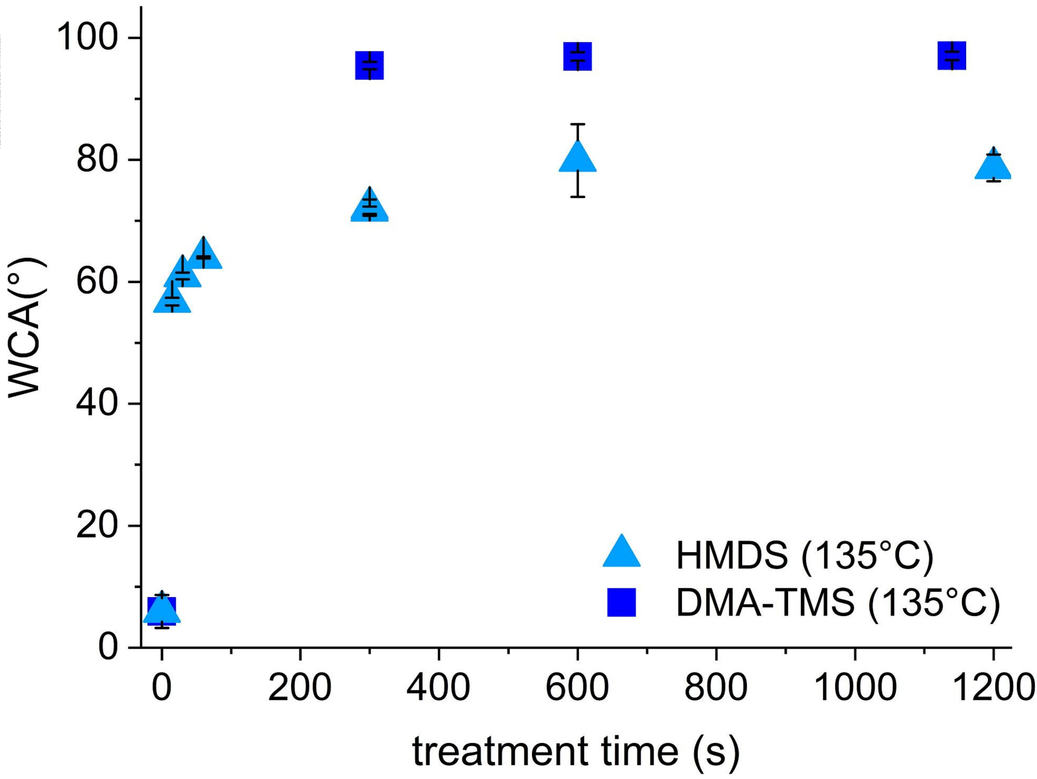

(b)

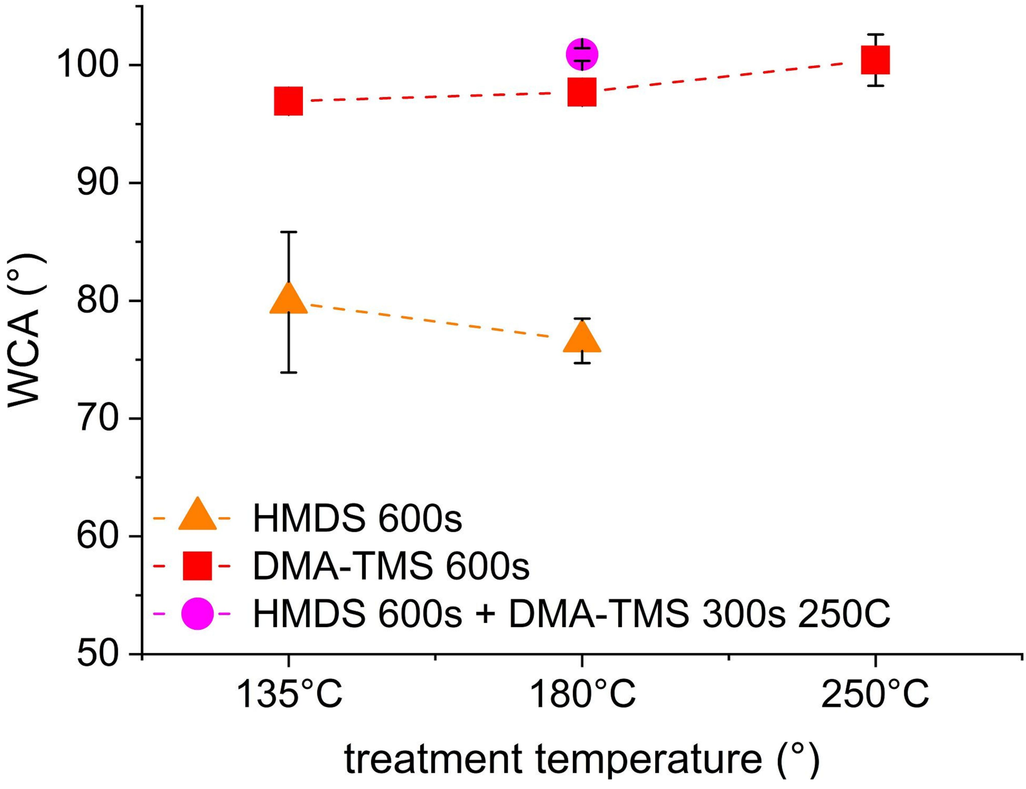

(c)

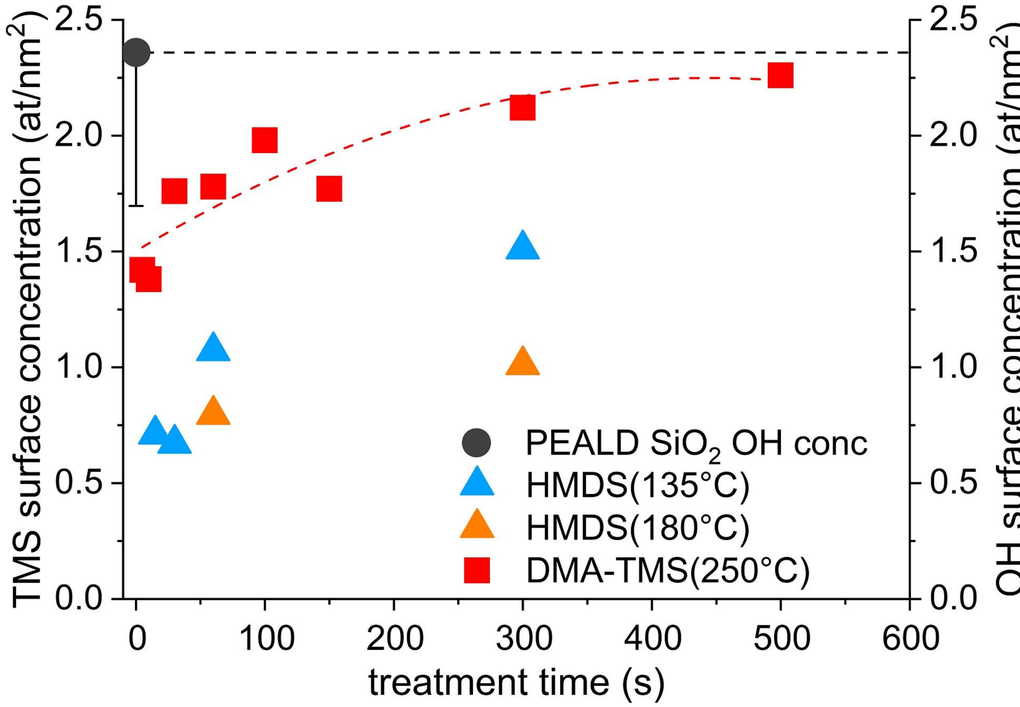

ACCEPTED MANUSCRIPT
Journal of Vacuum Science & Technology A
This is the author's peer reviewed, accepted manuscript. However, the online version of record will be different from this version once it has been copyedited and typeset.
PLEASE CITE THIS ARTICLE AS DOI: 10.1116/6.0002347

(a)

PEALD SiO_2
HMDS (135°C, 300s)
DMATMS (135°C, 300s)
DMATMS (180°C, 300s)
DMA-TMS (250°C, 300s)
HMDS (180°C, 300s) + DMA-TMS (250°C, 300s)

TiO_2 coverage (10^{15} at/cm^2)

TiO_2 ALD cycles

eq. TiO_2 thickness (nm)

(b)

Selectivity

TiO_2 thickness on SiO_2 (nm)

ACCEPTED MANUSCRIPT
Journal of Vacuum Science & Technology A
This is the author's peer reviewed, accepted manuscript. However, the online version of record will be different from this version once it has been copyedited and typeset.
PLEASE CITE THIS ARTICLE AS DOI: 10.1116/6.0002347

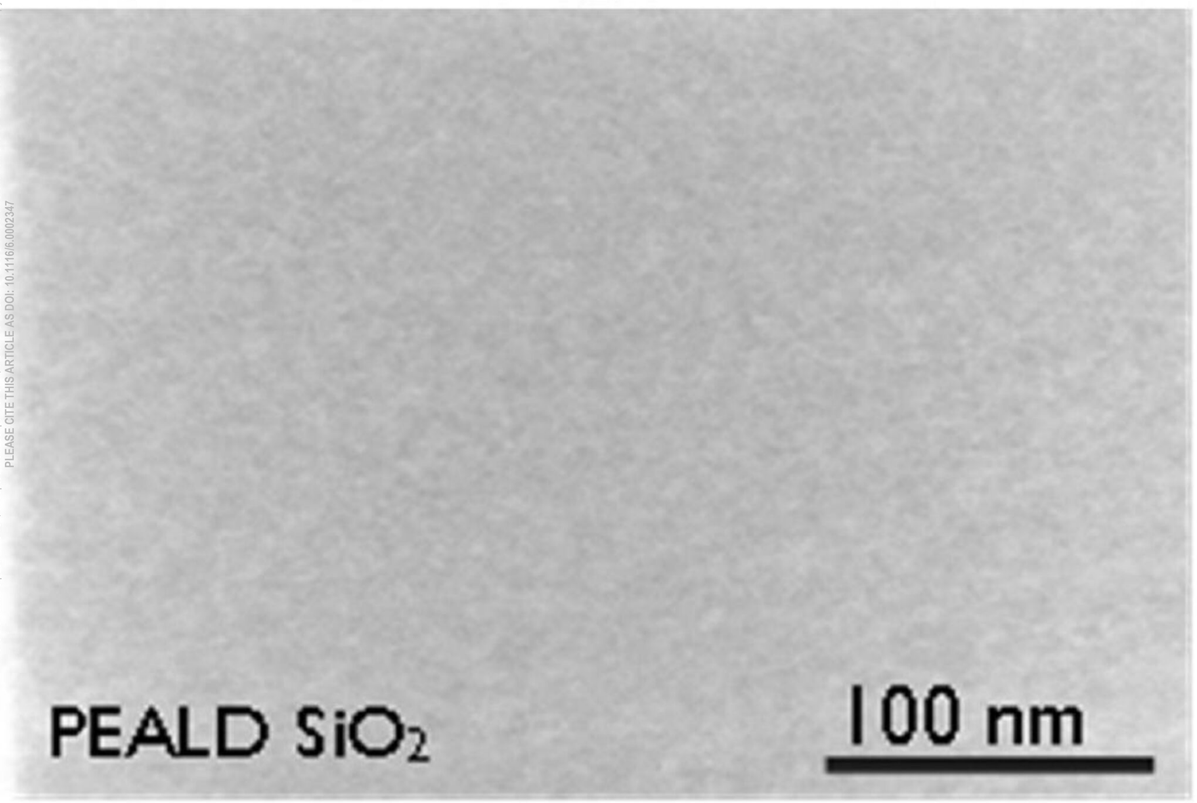

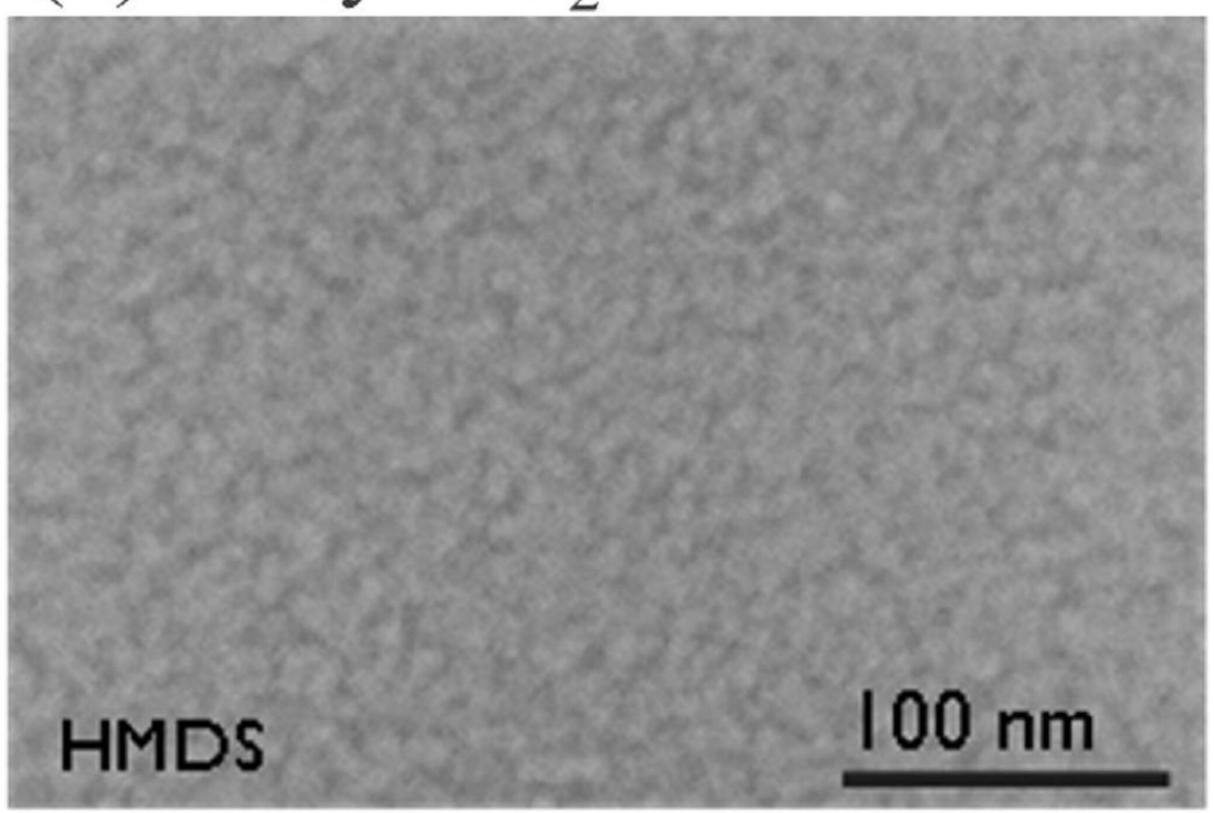

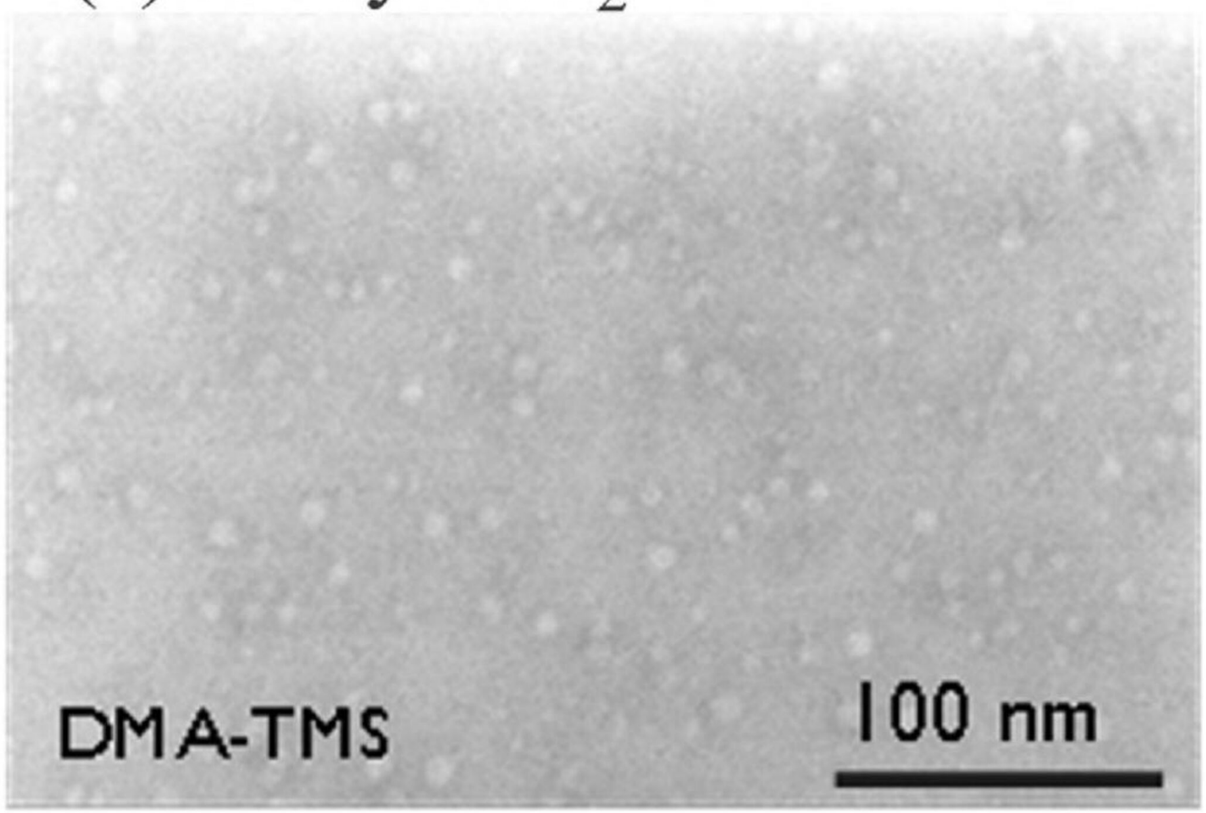

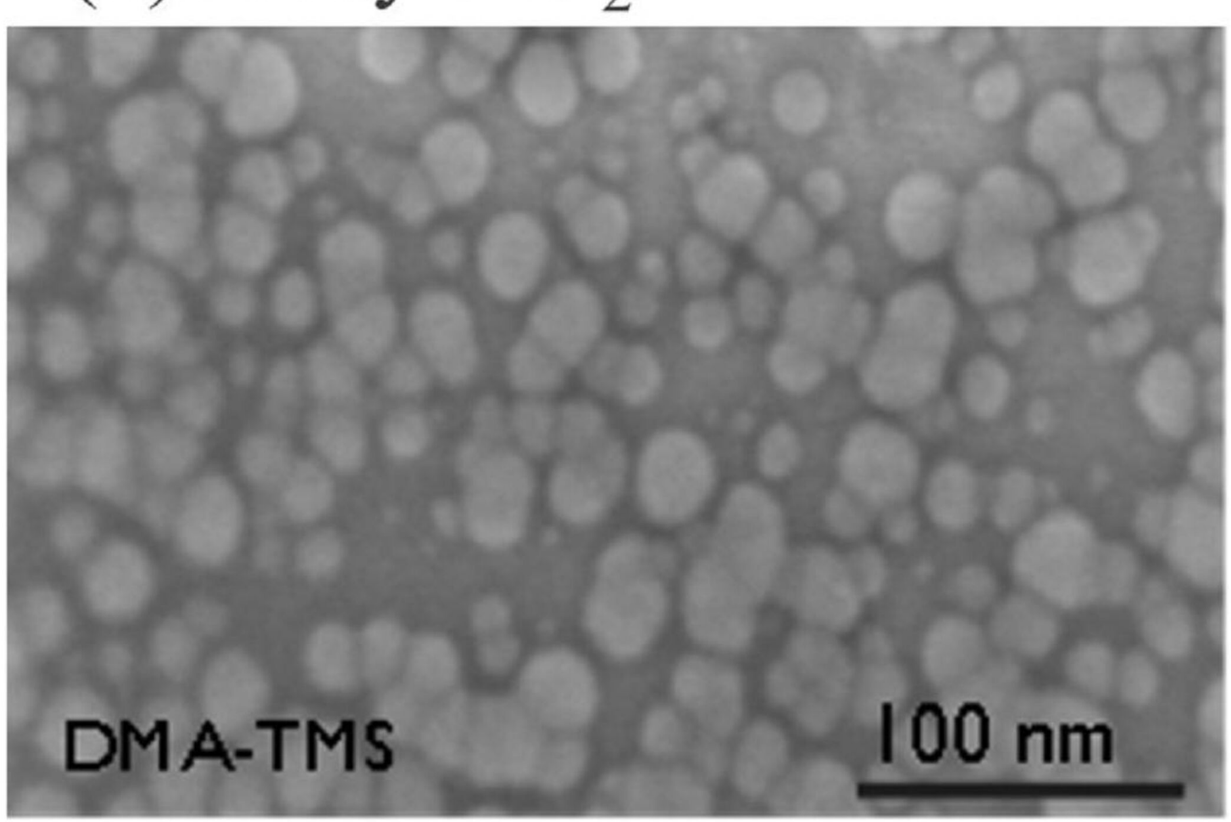

ACCEPTED MANUSCRIPT

Journal of Vacuum Science & Technology A

This is the author's peer reviewed, accepted manuscript. However, the online version of record will be different from this version once it has been copyedited and typeset.
PLEASE CITE THIS ARTICLE AS DOI: 10.1116/6.0002347

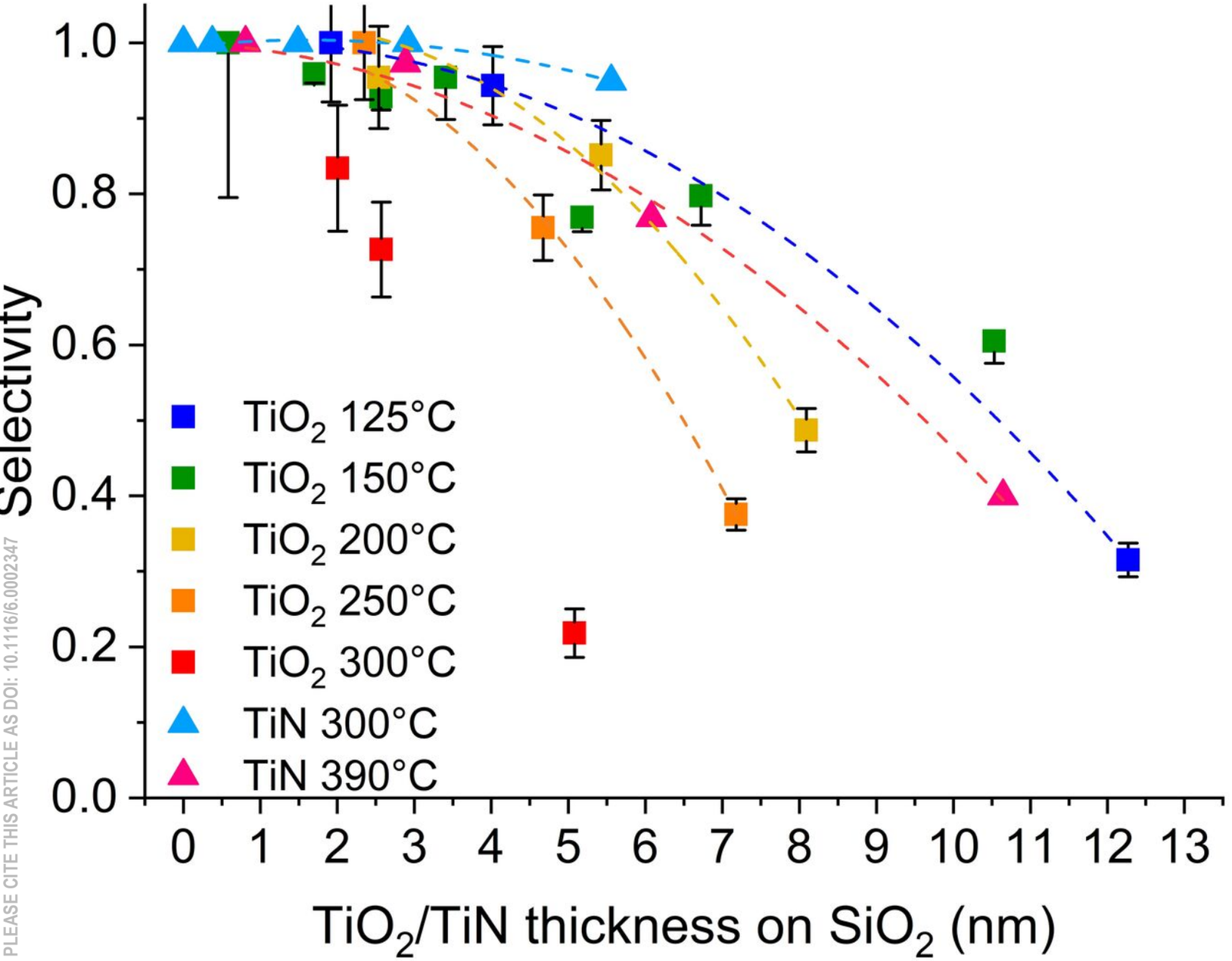

ACCEPTED MANUSCRIPT
Journal of Vacuum Science & Technology A
This is the author's peer reviewed, accepted manuscript. However, the online version of record will be different from this version once it has been copyedited and typeset.
PLEASE CITE THIS ARTICLE AS DOI: 10.1116/6.0002347

(a)

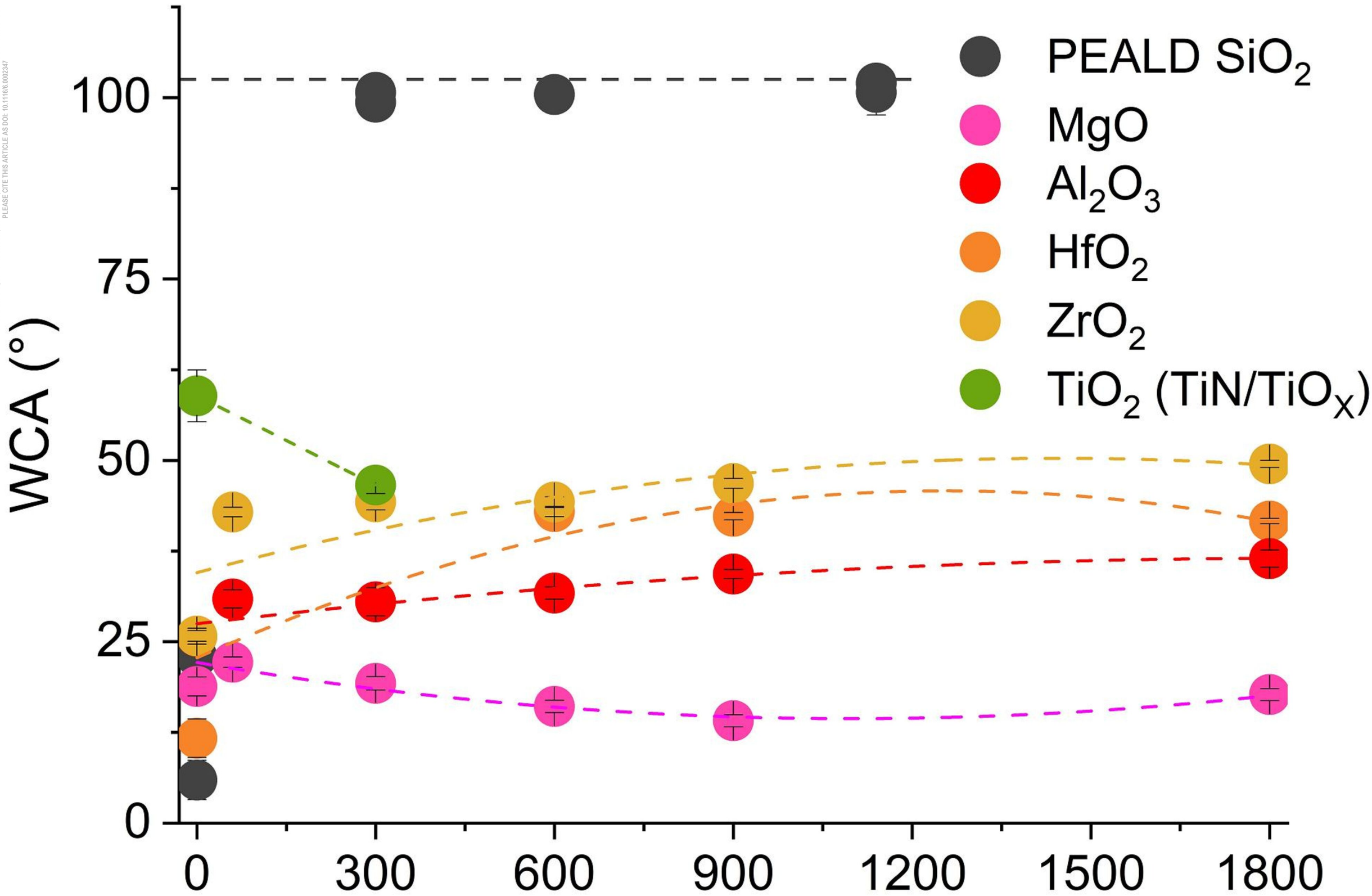

(b)

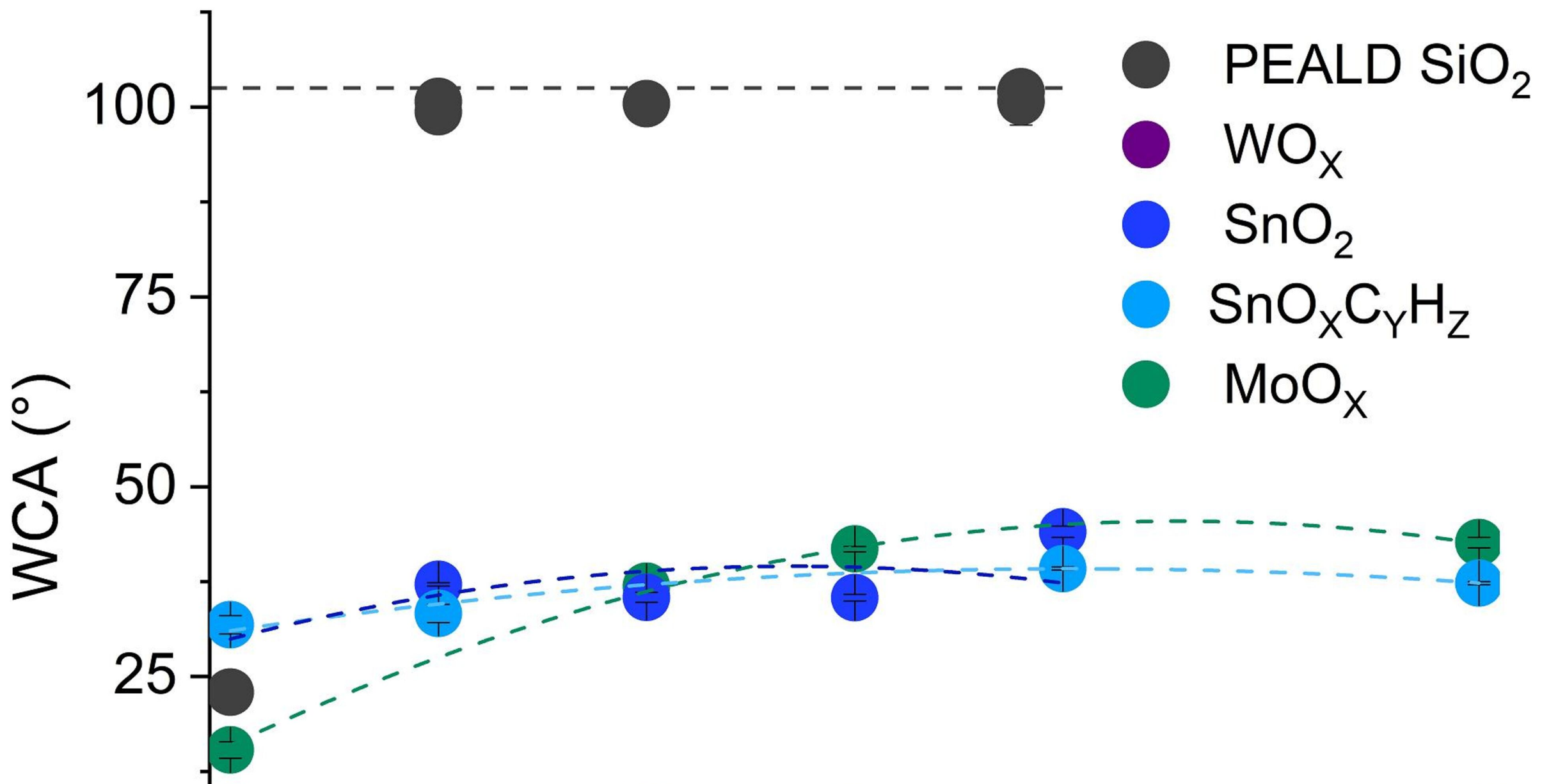

ACCEPTED MANUSCRIPT
Journal of Vacuum Science & Technology A

(a)

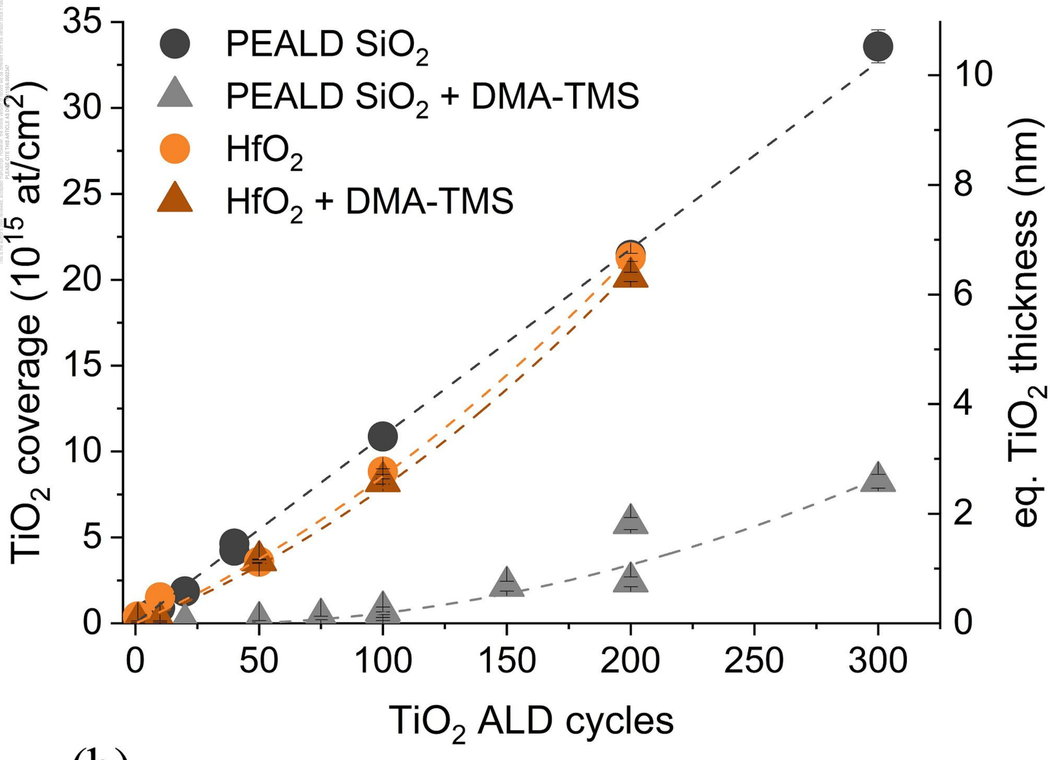

(b)

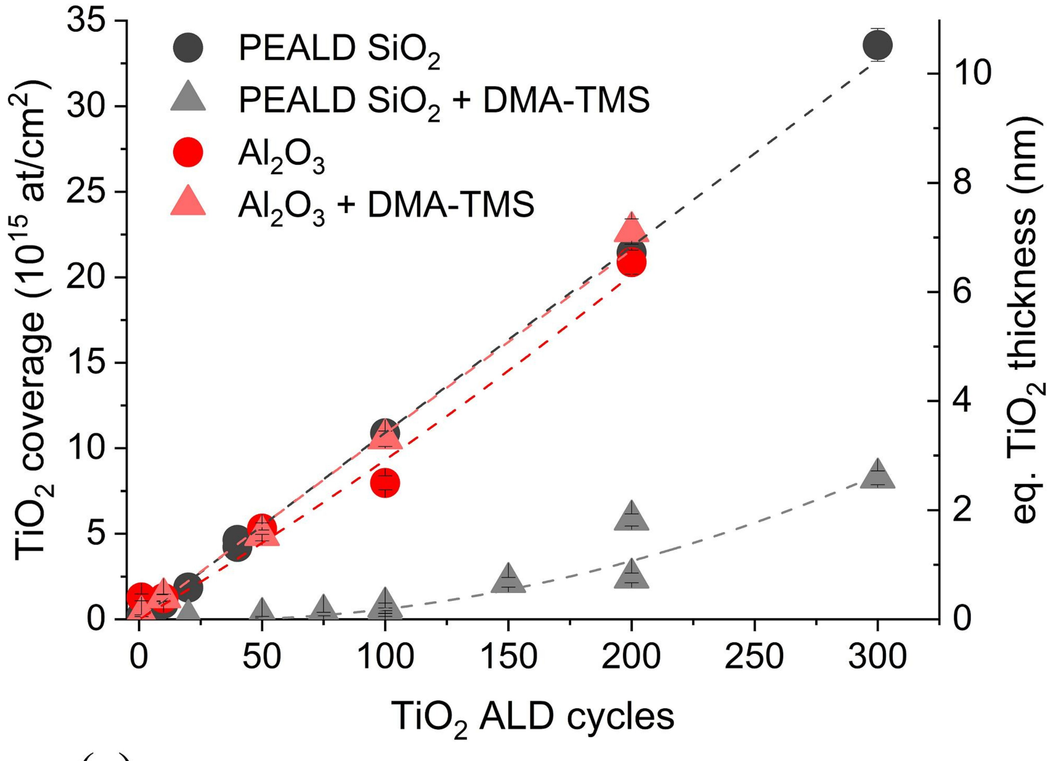

(c)

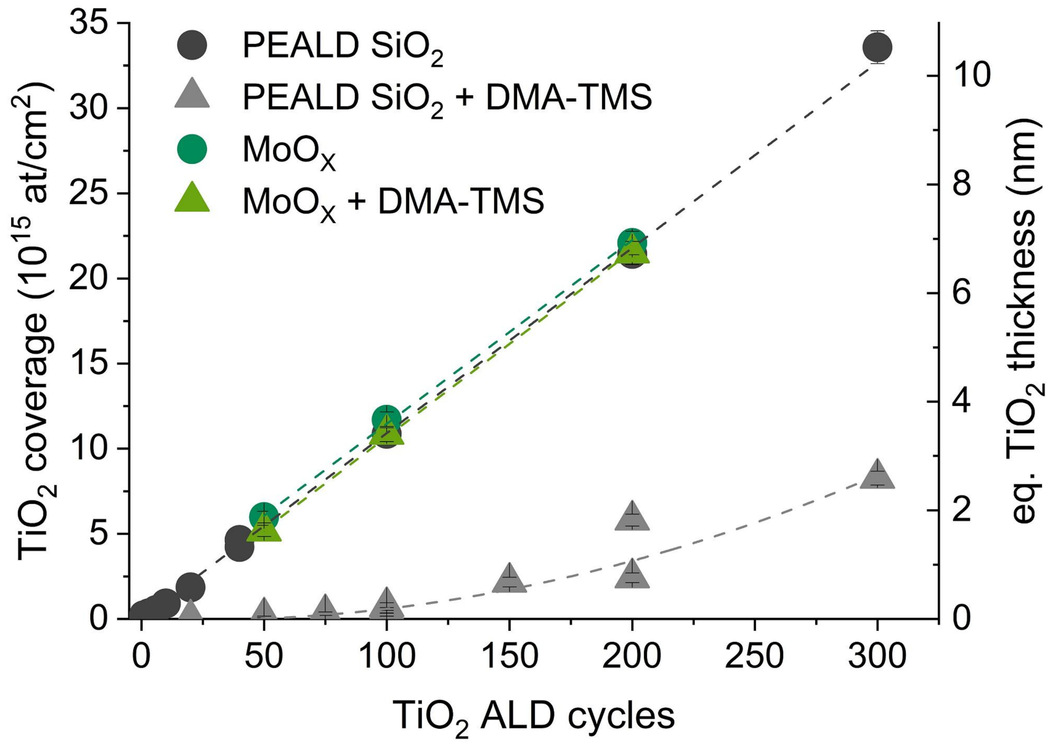

ACCEPTED MANUSCRIPT
Journal of Vacuum Science & Technology A
This is the author's peer reviewed, accepted manuscript. However, the online version of record will be different from this version once it has been copyedited and typeset.
PLEASE CITE THIS ARTICLE AS DOI: 10.1116/6.0002347

(a) SnO_2

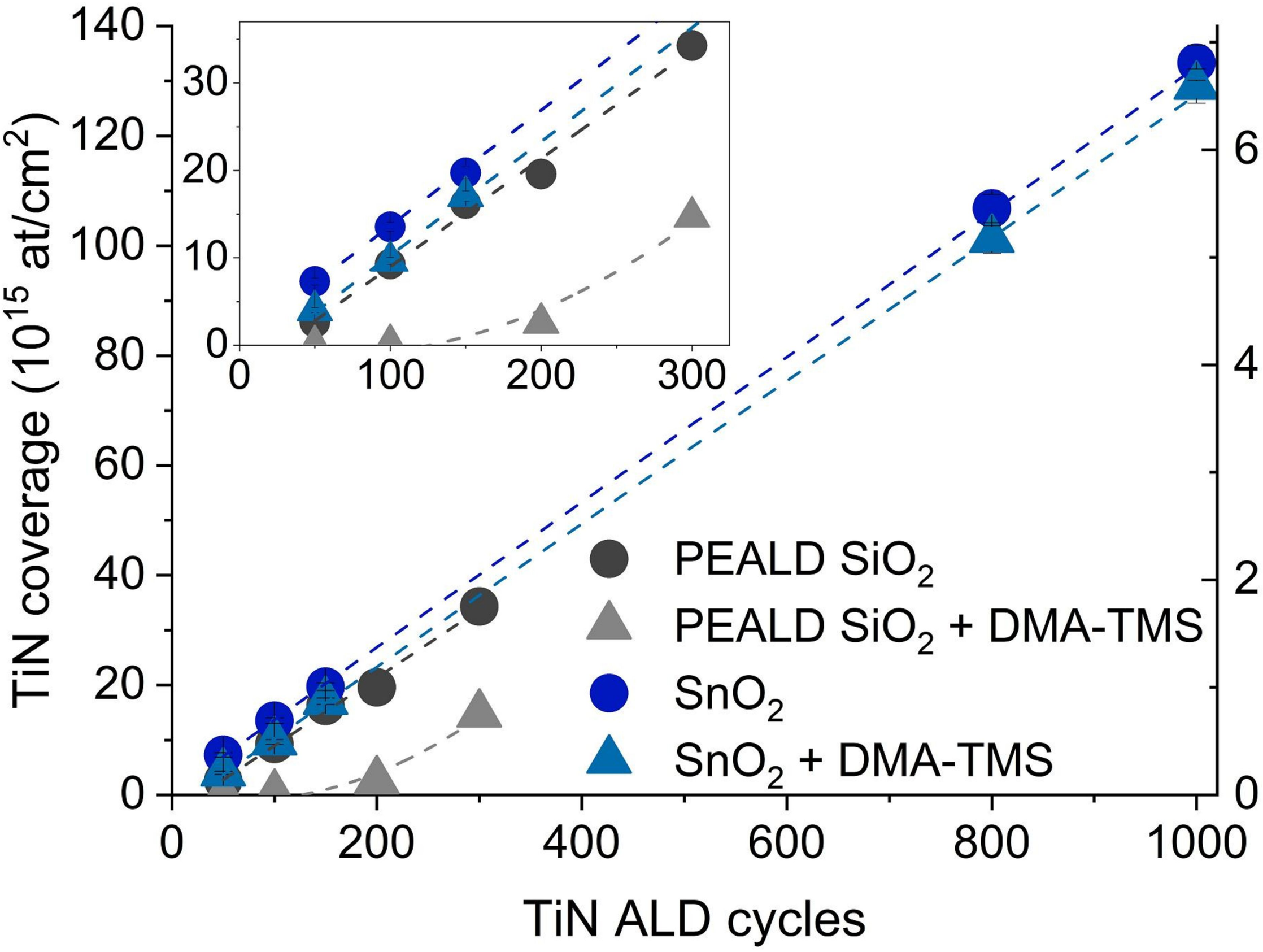

(b) $SnO_XC_YH_Z$

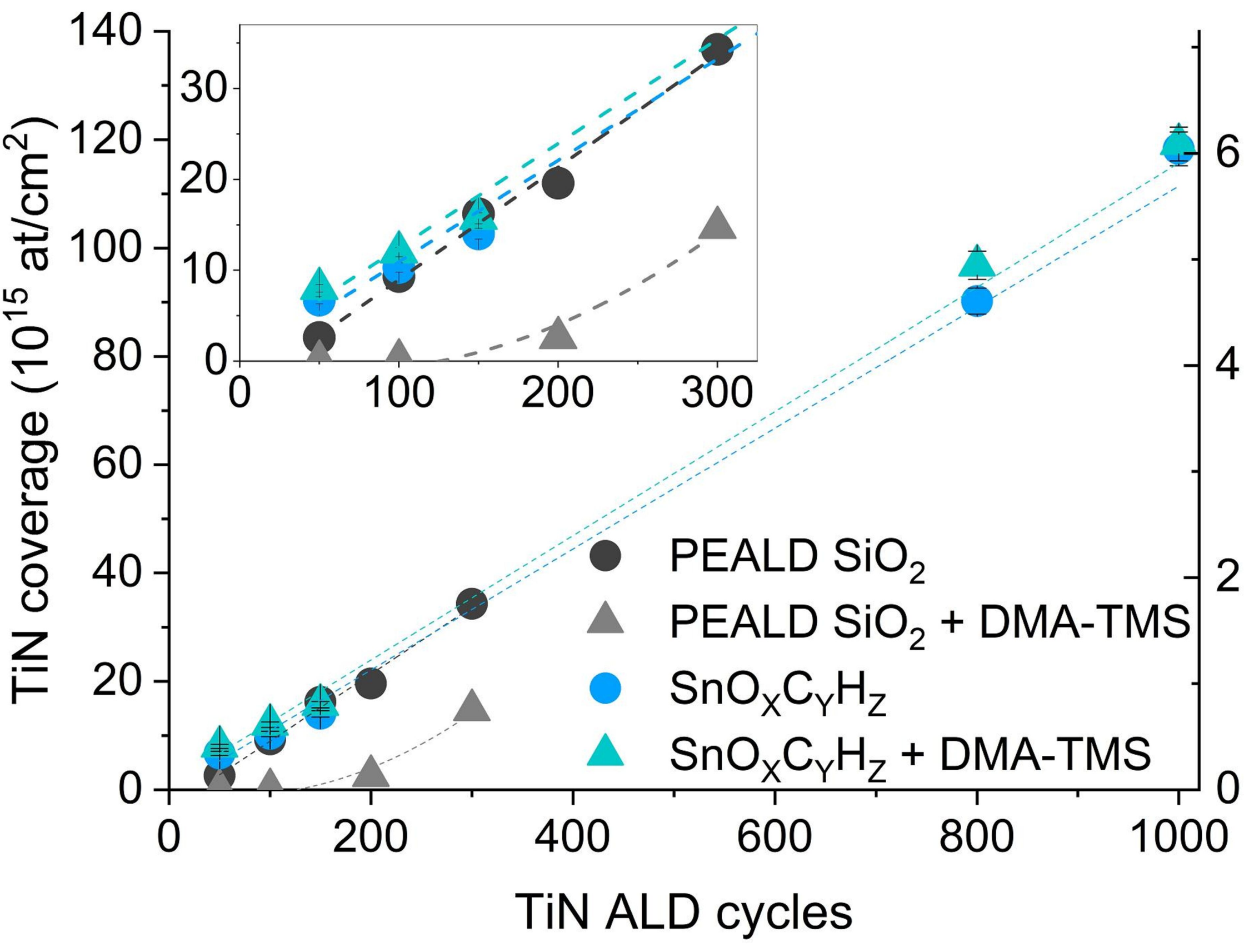

ACCEPTED MANUSCRIPT

Journal of Vacuum Science & Technology A

This is the author's peer reviewed, accepted manuscript. However, the online version of record will be different from this version once it has been copyedited and typeset.
PLEASE CITE THIS ARTICLE AS DOI: 10.1116/6.0001014

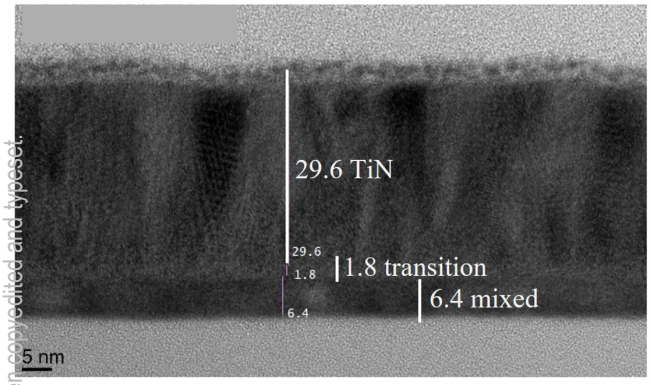

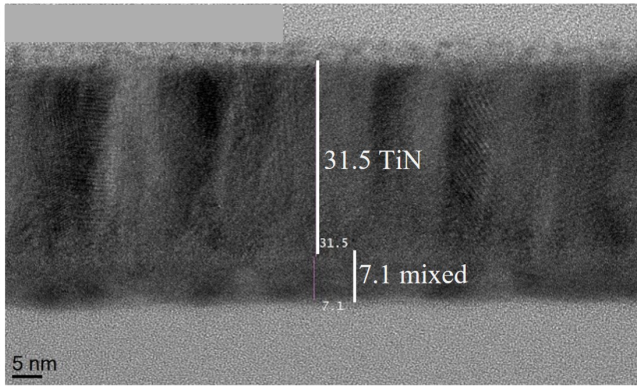

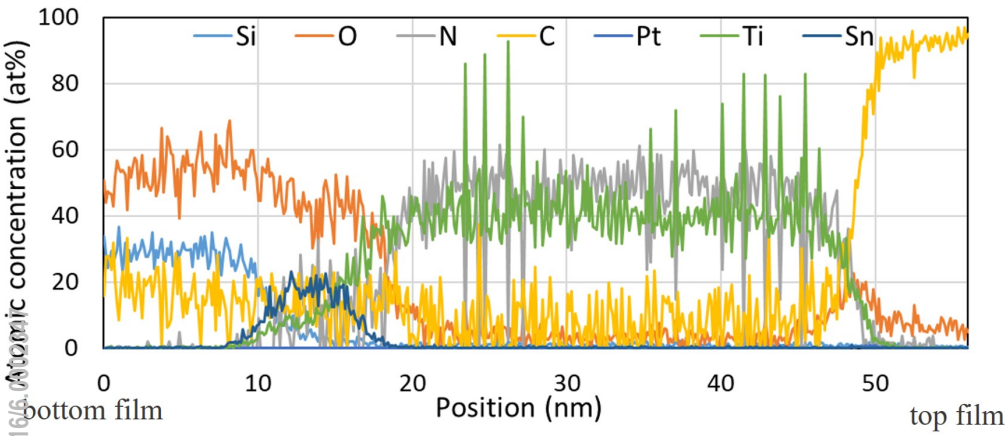

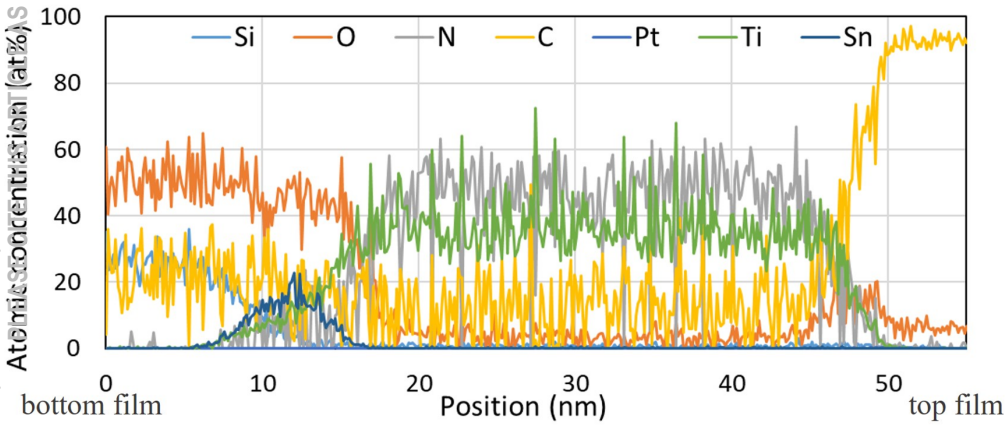

ACCEPTED MANUSCRIPT
Journal of Vacuum Science & Technology A
This is the author's peer reviewed, accepted manuscript. However, the online version of record will be different from this version once it has been copyedited and typeset.
PLEASE CITE THIS ARTICLE AS DOI: 10.1116/6.0002347

(a) $SnO_XC_YH_Z$

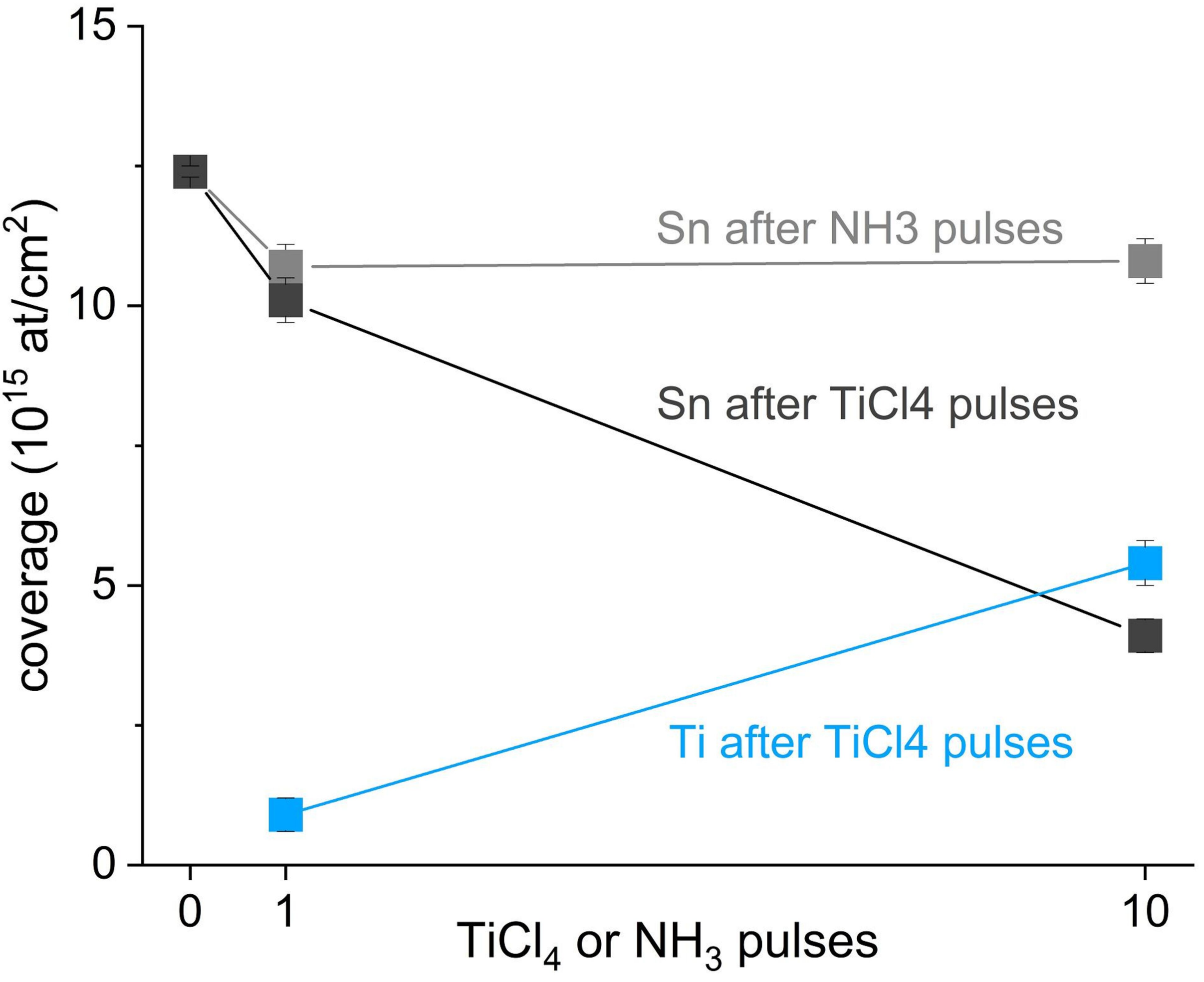

(b) SnO_2